INFLUENCE OF BOREHOLE CONSTRUCTION ON LNAPL THICKNESS MEASUREMENTS

By

JENNIFER L. THORSTAD

Bachelor of Science in Geology

North Dakota State University

Fargo, ND

2005

Submitted to the Faculty of the
Graduate College of the
Oklahoma State University
in partial fulfillment of
the requirements for
the Degree of
MASTER OF SCIENCE
May, 2007

INFLUENCE OF BOREHOLE CONSTRUCTION

ON LNAPL THICKNESS MEASUREMENTS

Thesis Approved:

Dr. Todd Halihan
Thesis Advisor

Dr. Anna Cruse

Dr. Eliot Atekwana

Dr. A. Gordon Emslie
Dean of the Graduate College

ACKNOWLEDGEMENTS

This research would not have been possible without the data provided by Aestus, LLC, Oklahoma Corporation Commission-Petroleum Storage Tank Division, and previous research conducted by the School of Geology at Oklahoma State University. Funding assistance from Devon Energy is also greatly appreciated.

I am especially grateful to my advisor, Dr. Todd Halihan, for pushing me to new limits. He provided valuable insight on numerical modeling, contaminant transport in the subsurface, and geophysical techniques. I also would like to thank my committee members, Dr. Anna Cruse and Dr. Eliot Atekwana, for critiquing my writing and always offering advice. Finally, I express my sincere gratitude to my family and friends for their support.

TABLE OF CONTENTS

LIST OF TABLES

LIST OF FIGURES

LIST OF SYMBOLS

Symbol	Description	Units
α	van Genuchten fitting parameter	L^{-1}
A	Area	L^2
C_{nw}	Specific capacity of non-wetting fluid	Dimensionless
C_p	Specific capacity, *p* denotes pressure	$LT^2 M^{-1}$
$C_{p,nw}$	Specific capacity of non-wetting fluid	$LT^2 M^{-1}$
$C_{p,w}$	Specific capacity of wetting fluid	$LT^2 M^{-1}$
C_w	Specific capacity of wetting fluid	Dimensionless
D	Coordinate of vertical elevation	L
dh/dL	Gradient	$L\ L^{-1}$
g	Acceleration of gravity	$L\ T^{-2}$
H_c	Capillary pressure head	L
K	Hydraulic conductivity	$L\ T^{-1}$
κ_{int}	Intrinsic permeability of porous media	L^2
$k_{r,nw}$	Relative permeability of wetting fluid	Dimensionless
$k_{r,w}$	Relative permeability of non-wetting fluid	Dimensionless
L	van Genuchten fitting parameter	Dimensionless
m	van Genuchten fitting parameter	Dimensionless
n	van Genuchten fitting parameter	Dimensionless

η_{nw}	Dynamic viscosity of non-wetting fluid	$M\ L^{-1}T^{-1}$
η_w	Dynamic viscosity of wetting fluid	$M\ L^{-1}T^{-1}$
p_c	Capillary pressure	$M\ L^{-1}T^{-2}$
p_{nw}	Pressure of non-wetting fluid	$M\ L^{-1}T^{-2}$
p_w	Pressure of wetting fluid	$M\ L^{-1}T^{-2}$
Q	Discharge	$L^3\ T^{-1}$
Se_{nw}	Effective saturation of non-wetting fluid	Dimensionless
Se_w	Effective saturation of wetting fluid	Dimensionless
t	Time	T
μ	Dynamic viscosity	$M\ L^{-1}T^{-1}$
ρ_{nw}	Density of non-wetting fluid	$M\ L^{-3}$
ρ_w	Density of wetting fluid	$M\ L^{-3}$
$\theta_{r,w}$	Residual porosity of wetting fluid	Dimensionless
$\theta_{r,nw}$	Residual porosity of non-wetting fluid	Dimensionless
θ_s	Total porosity	Dimensionless
$\theta_{s,nw}$	Total porosity of non-wetting fluid	Dimensionless
$\theta_{s,w}$	Total porosity of wetting fluid	Dimensionless
θ_w	Porosity or volume fraction of wetting fluid	Dimensionless

CHAPTER I

INTRODUCTION

Surface spills and leaky underground storage tanks containing light non-aqueous phase liquids (LNAPL) are a common source of ground water contamination. A LNAPL is a liquid such as gasoline that is less dense and largely immiscible with water. Therefore, LNAPL exists as a separate phase from water. Determining the lateral and vertical extent of the LNAPL below the ground surface is crucial to effectively remediate a contaminated site (LaBrecque et al., 1996). Commonly, the distribution of LNAPL in the natural media is determined from monitoring wells by assuming that the well and media are in equilibrium. A linear relationship is used to extrapolate the LNAPL thickness to the media (van Dam, 1967). However, Farr et al. (1990) and Lenhard and Parker (1990) both determined that there is no linear relationship between the LNAPL thickness in a monitoring well and the surrounding porous media.

Geophysical methods are thus needed to accurately determine the extent of LNAPL distribution at a contaminated site (Kemblowski and Chiang, 1990). Over the last 10 years electrical resistivity imaging (ERI) has become a sophisticated geophysical tool as seen through studies conducted by Daily et al. (1995); Benson and Mustoe (1996); Atekwana et al. (2000); Delaney et al. (2001); and Halihan et al. (2005a). Electrical resistivity images obtained at sites

contaminated with LNAPL often show the distribution of LNAPL affected by the location of boreholes in either an attractive or repulsive fashion (Halihan et al., 2005a). This will result in an anomalously low or high estimate of the amount of LNAPL in the formation using measurements from such wells.

Purpose of Study

This study examined the influence of borehole construction on LNAPL thickness measurements taken from monitoring wells. A numerical model was constructed to test the hypothesis that the hydraulic conductivity contrast between a borehole and natural media has a significant enough effect to create either a convergent or divergent two-phase flow field around a borehole. Such a flow field would lead to inaccurate LNAPL measurements in monitoring wells as compared to formation concentrations. Electrical resistivity images obtained from three sites contaminated by LNAPLs provide field evidence to test the hypothesis that the flow field is affected by the hydraulic conductivity contrast between the formation and the borehole.

Objectives

1. Evaluate the literature for the expected range of hydraulic conductivity values for borehole construction and natural media.
2. Evaluate the literature for studies conducted on the interaction of two-phase flow and wells.

3. Evaluate the literature for previous studies that apply electrical resistivity imaging to locate light non-aqueous phase liquids within the subsurface.

4. Numerically model the two-phase flow (LNAPL and water) interaction around a borehole within porous media under natural gradient conditions using COMSOL Multiphysics 3.3a.

5. Compare the model results to field data collected with electrical resistivity imaging surveys and core samples. Images were taken at three sites within Oklahoma that are contaminated by LNAPLs from leaky underground storage tanks.

Field Sites

Electrical resistivity surveys were conducted at three sites in Oklahoma (Figure 1.1) to identify LNAPLs that had leaked and migrated from underground storage tanks (UST). The Oklahoma Corporation Commission (OCC) Petroleum Storage Tank Division invited Oklahoma State University's (OSU) School of Geology to investigate the study sites in Golden and Enid, OK. The site in Enid was evaluated prior to and during remediation, while the site at Golden had already gone through remediation. Aestus, LLC, an environmental consulting firm out of Colorado, was contracted by the OCC to examine a commercial site in Hobart, OK that was in the preliminary site characterization phase.

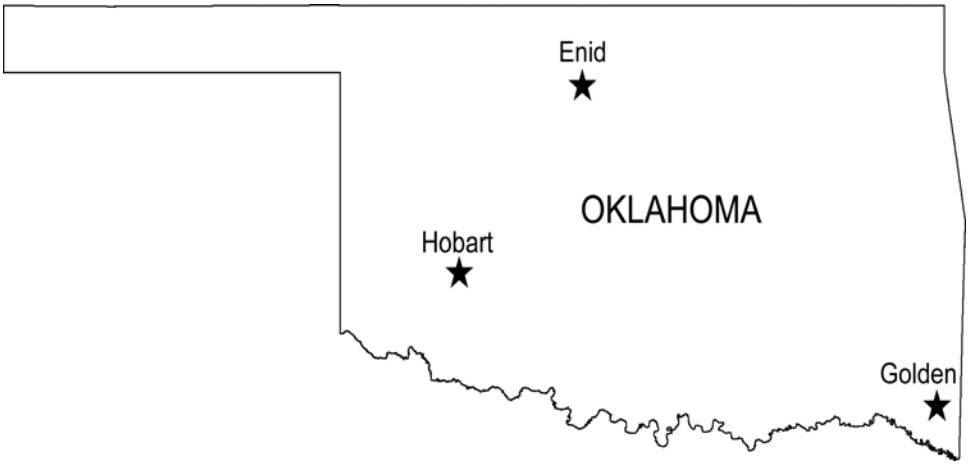

Figure 1.1: Location map of Enid, Golden, and Hobart, OK.

Field sites at Enid, Golden, and Hobart were chosen for this project because the sites are composed of similar unconsolidated sediments; sand, silt, clay, and gravel. The sediments at these sites are relatively conductive or low resistivity so fresh LNAPLs can be readily identified as resistive anomalies within the image. Geographically, the sites are located in different portions of Oklahoma with varying climates. The eastern half of Oklahoma is relatively moist compared to the western portion which is relatively dry. The average annual temperature increases from north to south (Johnson and Duchon, 1995).

Enid, OK

In 1996, a gas station located on 8th Street and Broadway in Enid, Oklahoma (Figure 1.2) was found to be leaking LNAPL into the subsurface from an underground storage tank (UST). The UST was excavated from the ground however; the LNAPL plume had already mobilized. McSorley (2003) used direct push electrical resistivity tomography to determine the distribution of the LNAPL

within the subsurface. The stratigraphy of the site was constructed by McPhail (2003) from 16 cores and electrical conductivity (EC) logs.

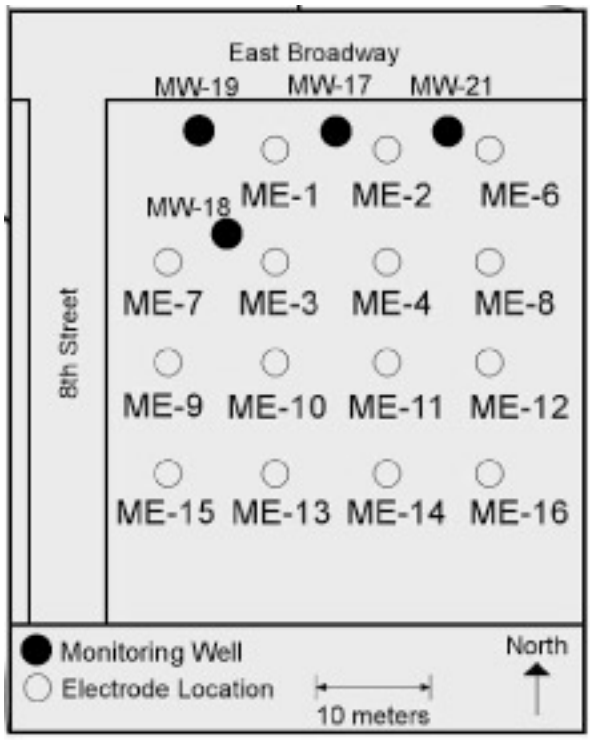

Figure 1.2: Location map of monitoring electrode boreholes at Enid, OK site (modified from McSorley, 2003).

Geology

The site consists of a vacant lot located across the street from a gas station. The lot is relatively flat lying and is approximately 50x50 meters. The LNAPL plume, as delineated by standard monitoring wells, was located in the north-central portion of the monitoring area, approximately 9 - 12 meters below the land surface (McSorley, 2003).

The geology of the site includes Quaternary alluvium and soil lying on Permian bedrock. The Quaternary sediment is divided into three units which are

composed of silty-sandy clay, gley, and sand with gravel (Table 1.1). The sand unit is water bearing and varies in thickness. Water levels range from 9.15 - 9.75 meters (30 - 32 feet) below the land surface. The Permian bedrock consists of red-brown shale with calcitic deposits (McPhail, 2003).

Unit	Unit Name	Thickness (ft)	Thickness (m)
C	Silty clay with sand	3 - 7	0.92 - 2.13
B	Sandy clay	25 - 29	7.62 - 8.84
	Gley	4 - 5	1.22 - 1.52
A	Sand-gravel	2.5 - 10.5	0.762 - 3.2
	Bedrock	Permian Hennessey Group	

Table 1.1: Stratigraphy of the Enid, OK site (modified from McPhail, 2003).

Field Data

Electrical resistivity tomography (ERT) images (Figure 1.3) were taken during July and August 2003. The line was 20 meters long and ran south to north from monitoring electrodes (ME) 13, 10, and 3 (Figure 1.2). The resistivity of this image ranged from 1 - 52 ohm-meters. The top profile in Figure 1.3 was taken in July 2003 while pumping occurred on site. Following the electrical survey, cores were taken to confirm the location of LNAPL from the resistivity image. Total petroleum hydrocarbon (TPH) concentrations were measured in cores (Figure 1.3). The highest levels of TPH are present in the clay layer

(above the black line; Halihan et al., 2005c). The bottom image in Figure 1.3 was collected in August 2003 to monitor the progress of the remediation efforts. Halihan et al. (2005c) found that through time the images indicated the material had become more conductive which implied less LNAPL. No data regarding LNAPL thickness were obtained from the electrode boreholes when these images were collected. However, monitoring wells near the ERT ME 13-10-3 indicated a decrease in LNAPL thickness measurements over time with the exception of MW - 18 (Figure 1.4).

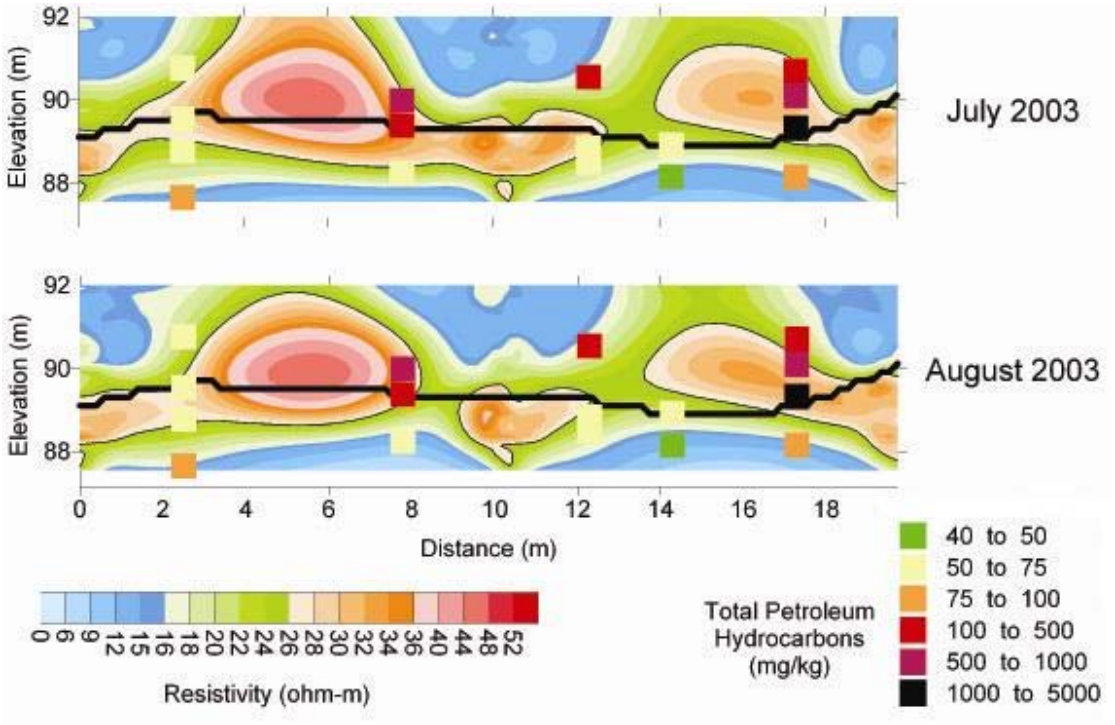

Figure 1.3: ERT compared to TPH along ME 13-10-3 at Enid, OK site. Black line represents boundary between clay and sand (adapted from Halihan et al., 2005c).

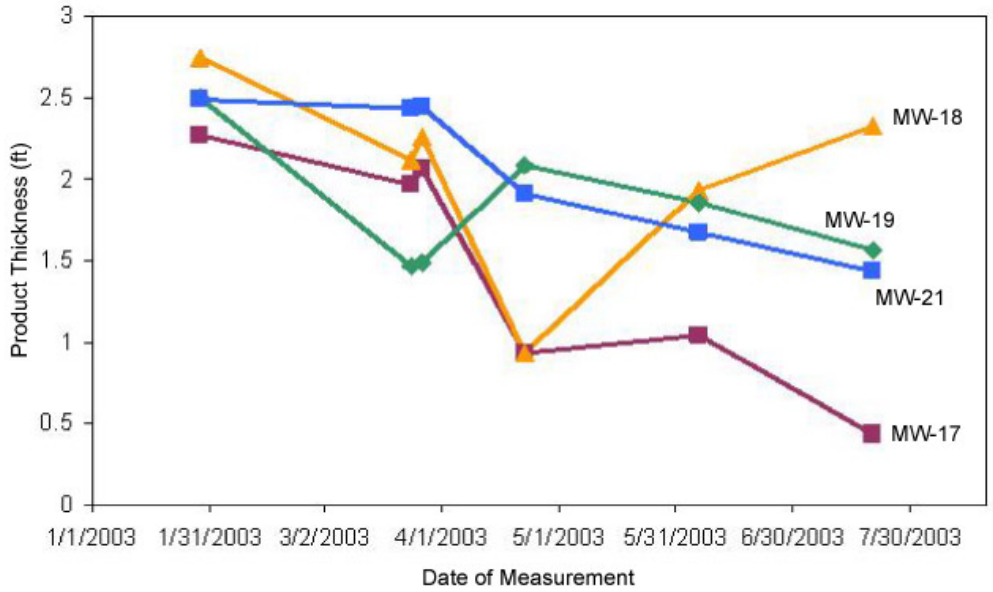

Figure 1.4: LNAPL thickness measurements from wells at Enid, OK site (well data provided by OCC).

Golden, OK

In December of 1993, LNAPL was reported in a well on this site. The source was determined to be an above ground storage tank. In March of 1999, two leaky underground storage tanks were also located within the site. The tanks were removed and remediation of the LNAPL was performed (Graham, 2007). In March of 2003, OSU's School of Geology applied ERI and direct push techniques to aid the post-remediation evaluation of the site (Halihan et al., 2005b). Graham (2007) used a combination of surface and borehole electrodes to characterize subsurface conditions (Figure 1.5).

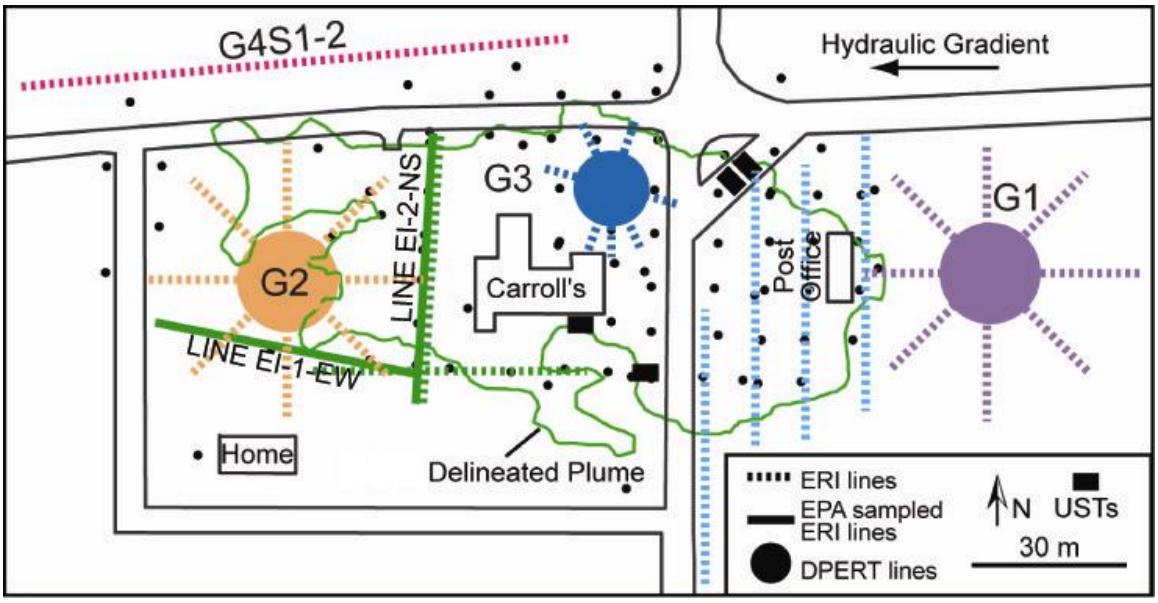

Figure 1.5: Map of well locations and electrical resistivity lines at Golden, OK (modified from Halihan et al., 2005b).

Geology

The Golden site is made up of two city blocks and is approximately 5000 m^2 (16,400 ft^2) in area. The geology consists of Quaternary alluvium overlying Cretaceous sand deposits. The alluvium is associated with the surrounding rivers and is composed of fining and coarsening upward sequences. The general stratigraphy of the site consists of clay, silt, sand, and gravels (Table 1.2). Five cores collected ranged in depth from 21.5 - 27.25 ft (6.55 - 8.31 m) were retrieved by direct push dual tube sampling. Water levels ranged from 384 - 394 ft relative to mean sea level at depths of 10 - 15 ft below land surface. The hydraulic gradient flows from east to west (Graham, 2007).

Unit Name	Thickness (ft)	Thickness (m)
Silty, Gravelly Soil	0.25 - 1.5	0.076 - 0.46
Sandy-Silty Clay	11.75 - 13.5	3.58 - 4.11
Sandy-Clayey-Silty Gravel	6.25 - 9.75	1.9 - 2.97
Silty-Clayey Sand	5.75 - 7.5	1.75 - 2.3

Table 1.2: Stratigraphy of the Golden, OK site (adapted from Graham, 2007).

Field Data

An electrical resistivity image (G4S1-2) was taken on the northwestern portion of the site; outside of the delineated LNAPL plume (Figure 1.6). Figure 1.6 represents the background of the site since no resistive anomalies are seen in the image, indicating no LNAPL contamination. The line was run 350 ft long and imaged to a depth of 40 ft. Resistivity ranged from 15 - 252 ohm-m. Halihan et al. (2005b) interpreted the stratigraphy of this image to consist of clay (light blue) from 0 - 20 ft and the clayey gravel (green-yellow) from 20 - 40ft.

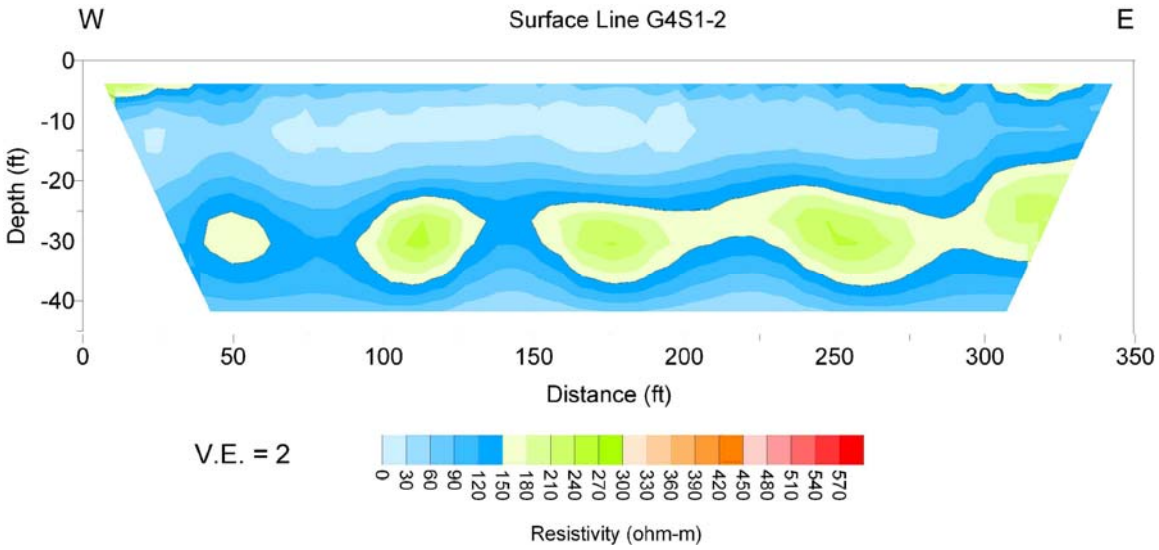

Figure 1.6: Electrical resistivity image of subsurface at Golden, OK site (Halihan et al., 2005b). This image detects no LNAPL contamination.

ERI lines EI-1-EW and EI-1-NS were collected on the west side of the field site (Figure 1.5). EI-1-EW (Figure 1.7) was taken outside of the delineated plume boundary. Both lines were 50 m long and imaged to a depth 10 m. Resistivity ranged from 2 - 1750 ohm-m. Image EI-1-EW depicts a single resistive anomaly that extends vertically from near the surface to 6 m depth and extends horizontally for 20 m. The center of the anomaly was cored by the EPA. The maximum concentration of hydrocarbon present in the sample core was 60.8 mg/kg (Halihan et al., 2005a).

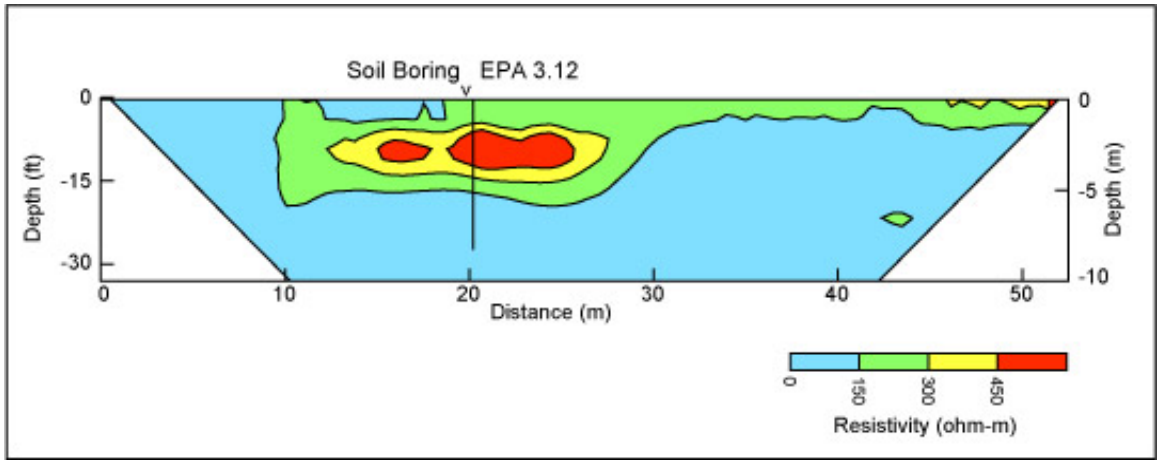

Figure 1.7: ERI taken along line EI-1-EW at Golden, OK site (Halihan et al., 2005a). Vertical line represents the location of core sample.

Image EI-2-NS (Figure 1.8) was located both inside and outside of the delineated plume. Three major resistive anomalies are present in profile A. All three resistive anomalies are seen as discontinuous, discrete zones or “blobs”. The lateral extent of the anomalies ranges from 5 - 10 m and vertically extends 4 - 5 m. Soil cores were taken by the EPA (Figure 1.8, Profile B) to confirm the resistivity images, measured TPH concentrations range between non-detect and 21,300 mg/kg. The highest concentration of TPH was observed in soil boring EPA 3.10 and the lowest value of TPH was measured in EPA 3.13, 3.14, and 3.16 (Figure 1.8B; Halihan et al., 2005a). There was no free product detected in the monitoring and remediation wells indicated in EI-2-NS (Figure 1.8 A, B).

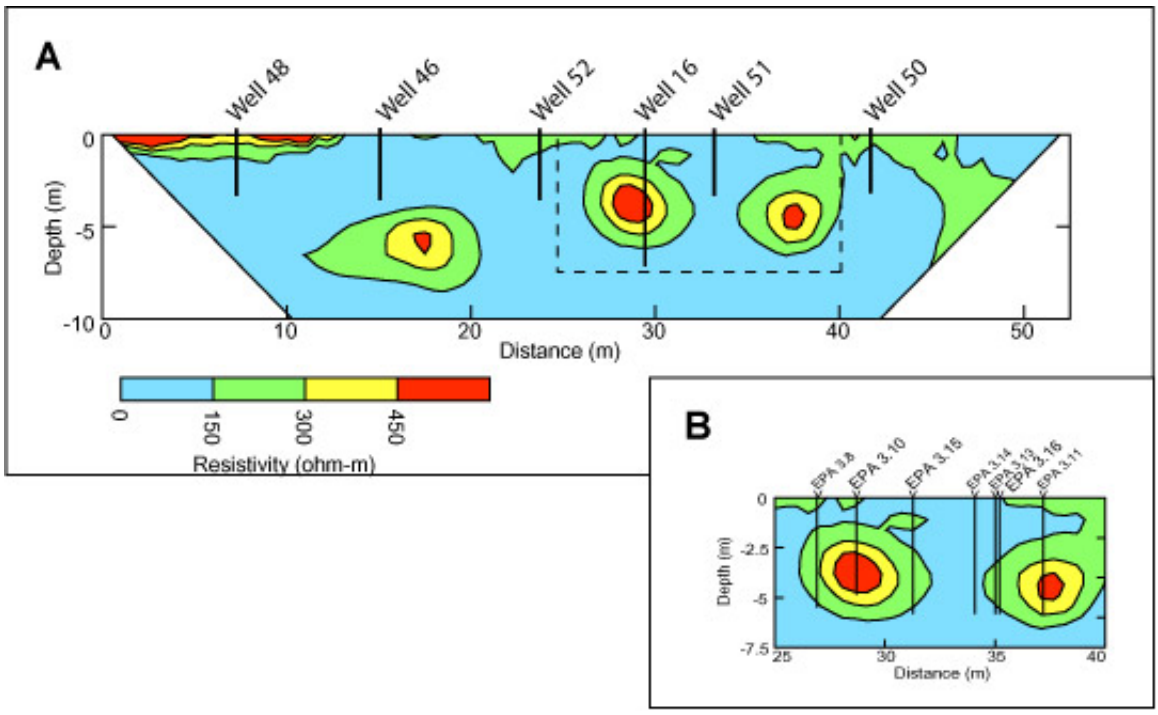

Figure 1.8: ERI taken along line EI-2-NS at Golden, OK site (modified from Halihan et al., 2005a). Profile A shows the ERI with locations of monitoring and remediation wells. Well 16 is an extraction well. Wells 48, 46, 52, and 50 are injection wells. Profile B is an enlarged image of the dotted area in Profile A. Profile B depicts the locations of soil borings.

Hobart, OK

In 2004, Aestus, LLC, conducted electrical resistivity surveys to locate LNAPLs within the subsurface at the Department of Human Health Services site in Hobart, OK (Figure 1.9). Aestus located the LNAPL using their proprietary GeoTrax Survey™ technology.

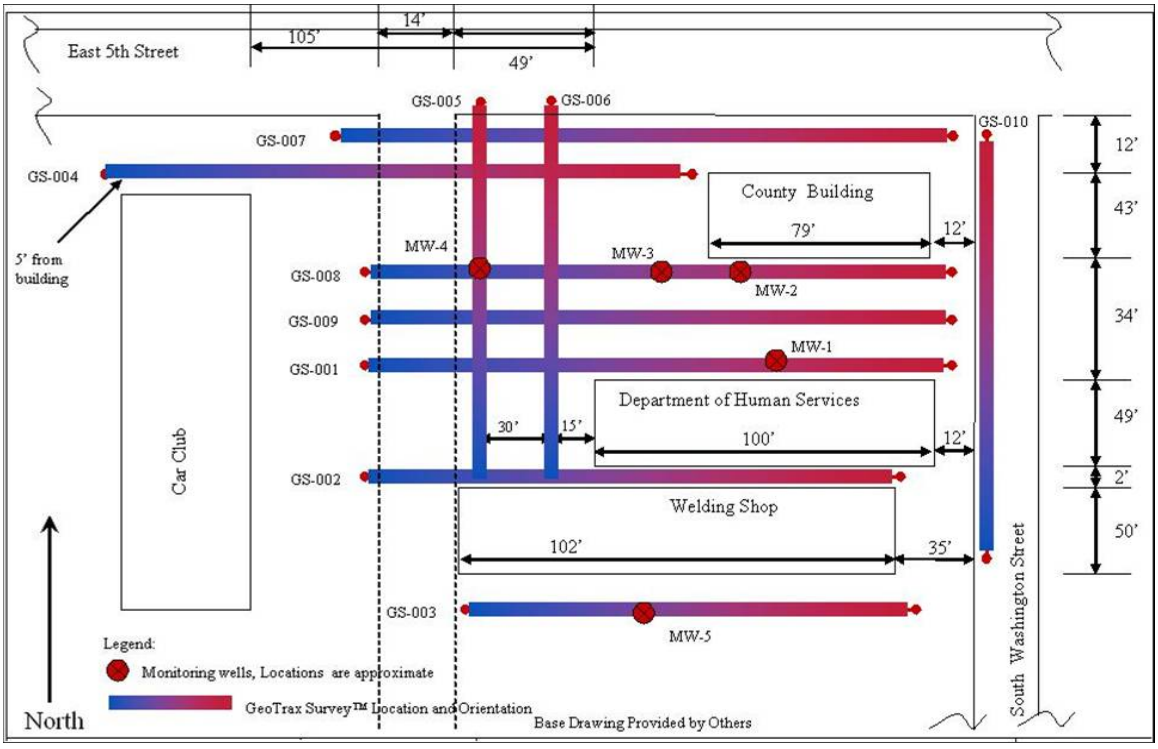

Figure 1.9: Map of well locations and electrical resistivity lines at Hobart, OK site (Aestus, 2004).

Geology

The site is located within a commercial area in the town of Hobart, OK which limits the subsurface access. The site consists of four buildings which are surrounded by streets. The area where the resistivity surveys were conducted is approximately 250 x 200 ft (76.2 x 61 m). Overall, the site is relatively flat lying with an average ground level elevation of approximately 100 ft (~30.5 m).

Based on soil borings collected by Secor (2004), the geology of the site consists of only of Quaternary alluvium. The alluvium is predominantly silty clay with thin claystone and gravel lenses lying beneath the silty clay (Table 1.3). See Appendix A for detailed lithologic descriptions. The water table in monitoring

wells (MW) 1 - 5 was approximately 12 ft (3.7 m) below the land surface. Ground water flows from east to west on this site (Figure 1.9).

Unit Name	Thickness (ft)	Thickness (m)
Silty Clay	~15 ft	4.6 m
Gravel	0.5 - 1.5 ft	0.15 - 0.46 m
Claystone	0.5 - 1 ft	0.15 - 0.3 m

Table 1.3: Stratigraphy of the Hobart, OK site
(adapted from Secor, 2004).

Field Data

ERI GS-008 (Figure 1.10) was taken in early August 2004 by Aestus, LLC. The line was 180 ft (54.9 m) long, and ran from west to east in the center of the site (Figure 1.9). The survey was performed on an asphalt parking lot. The image indicates the presence of two significant resistive anomalies as seen by the orange and red colors. Cores were drilled where the monitoring wells were located to determine if the resistive anomalies were LNAPLs. High values of total petroleum hydrocarbons were detected from the soil samples (Table 1.4). A photo ionization detector (PID) is a vapor and gas detector that measures the concentration of a variety of organic compounds. The highest PID readings were observed approximately 13 feet below the surface in the boring locations. Monitoring wells 2 and 4 (MW-2 and MW-4) were installed in the highly resistive areas and MW-3 was installed in less resistive zone that was located on an

asphalt patch (Aestus, 2004). No free product was detected in any of the wells (Table 1.5).

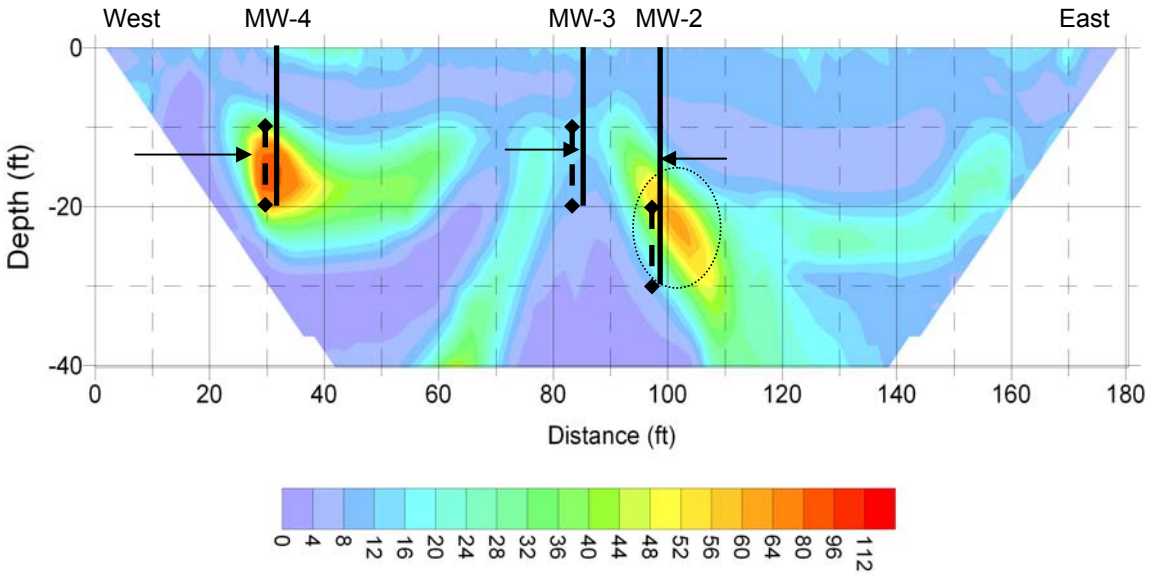

Figure 1.10: ERI of line GS-008 at Hobart, OK site (Aestus, 2004). Circle indicates area of significant anomaly. Dashed line indicates well screen interval. Solid line indicates soil boring interval. Arrow indicates the depth of highest PID reading. Resistivity scale is in ohm-meters.

Sample Point	Date	Sample Depth (ft)	TPH-GRO (mg/kg)	TPH-DRO (mg/kg)
MW-2	8/19/04	13.0 - 14.0	122	49
		14.0 - 15.0	200	45
MW-3	8/19/04	11.0 - 12.0	1030	103
		12.0 - 13.0	787	26
MW-4	8/19/04	12.0 - 13.0	311	22
		13.0 - 14.0	294	19

Table 1.4: Core data from Hobart, OK site (data provided by OCC). (TPH=total petroleum hydrocarbons; GRO= gasoline range organics; DRO=diesel range organics)

Monitoring Well	Date	Depth to Water (ft)	Depth to Product (ft)	Product Thickness (ft)
MW-2	9/1/04	20.34	NP	0
	11/11/04	11.20	NP	0
	10/11/05	10.86	NP	0
MW-3	9/1/04	11.49	NP	0
	11/11/04	11.12	NP	0
	10/11/05	10.62	NP	0
MW-4	9/1/04	11.61	NP	0
	11/11/04	11.27	NP	0
	10/11/05	10.75	NP	0

Table 1.5: Depth to ground water and LNAPL at Hobart, OK site (data provided by OCC). (NP= no product)

Summary

All three field sites were contaminated by leaky underground storage tanks which released LNAPL that subsequently migrated into the subsurface. LNAPL thickness measurements made in monitoring wells did not correlate with electrical resistivity images and direct TPH measurements from soil cores. Resistivity images taken at the Golden and Hobart sites showed resistive anomalies and soil boring confirmed the presence of LNAPL even when monitoring wells did not contain any product. The monitoring wells at the Enid site contained LNAPL, however the thickness in the well did not correlate with ERI and core samples. From these observations, we have developed the hypothesis that borehole construction influences LNAPL thickness measurements within a well. Consequently, LNAPL thickness measurements in wells may have little relationship to the quantity in the surrounding porous media.

CHAPTER II

REVIEW OF LITERATURE

A numerical model is constructed in this study to examine the influence of borehole construction on LNAPL thickness measurements. Therefore, a general description of borehole construction will be provided for both monitoring and pumping wells. Significant parameters and variables of the natural media and borehole construction will be explained. The basic theory of hydraulic conductivity as well as the known values for natural media and borehole construction materials will also be presented. These values will subsequently be used in the numerical model.

Previous efforts to model the volume estimation of hydrocarbon within porous media from fluid levels within a well will be reviewed. Studies performed to delineate LNAPL contamination within the subsurface through the use of electrical resistivity surveys will also be discussed. Finally, a previous study using COMSOL Multiphysics to model two-phase flow is described.

Borehole Construction

Monitoring Wells

Monitoring wells (Figure 2.1) are used to record head measurements in saturated media, sample ground water, and numerous other tests. Water flows

through the well screen and rises or falls until the hydraulic head between the natural media and well are equal. When properly designed, the well screen allows fluid to pass through and prevents sediments greater than the screen opening from entering into the well. Well screens are used in unconsolidated and semiconsolidated sediment (Charbeneau, 2000).

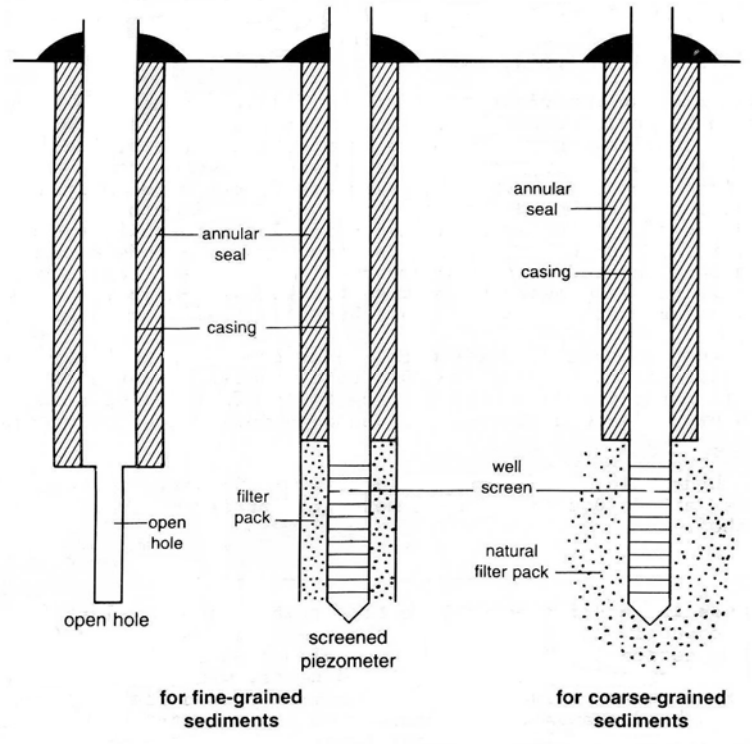

Figure 2.1: Construction of monitoring wells (Herzog, 1994).

A filter pack, also known as a gravel or sand pack, is commonly placed between the borehole wall and the screen to keep sediment out of the well screen. The well screen prevents approximately 90% of the filter pack from entering the well. Using a filter pack to retain the natural media increases the effective hydraulic diameter of the well by increasing the permeability (Driscoll, 1986).

An annular seal, typically consisting of bentonite, is placed between the well casing and borehole wall above the screened interval. The seal obstructs down hole movement of sediment and fluids within the natural media. The seal is poured or pumped onto the top of the filter pack material to isolate the zone from which the well is sampling (Weight and Sonderegger, 2001).

Pumping Wells

The main elements of a pumping well consist of the pump, casing and screen (Figure 2.2). The casing protects the pumping equipment which is housed inside the well. The screen, just like in monitoring wells, prevents sediment from entering the well, but allows fluid to pass through. Filter packs may also be used to make the zone around the screen more permeable.

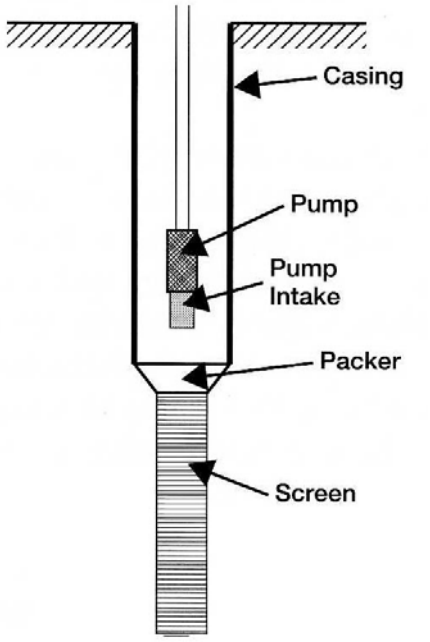

Figure 2.2: General configuration of a pumping well (Charbeneau, 2000).

Significant Parameters and Variables

Several significant parameters and variables must be considered to define flow within a two-phase system. These variables will be used in the numerical model generated for this study. The hydraulic conductivity values for natural media and borehole construction are presented first since all of the subsequent variables are allocated by this value.

Hydraulic Conductivity

Hydraulic conductivity as defined by Fetter (2001) is the coefficient of proportionality describing the rate at which water can be transmitted through porous media. This can be written mathematically as:

$$K = \frac{-Q}{A(dh/dL)} \tag{2.1}$$

where *K* is the hydraulic conductivity (L/T); *Q* is discharge (L^3/T); *A* is the cross-sectional area (L^2); and *dh/dL* is the gradient (L/L). Hydraulic conductivity also depends on the density and viscosity of the fluids flowing through the natural media (although when not defined, one generally assumes the fluid is water):

$$K = \frac{k \rho g}{\mu} \tag{2.2}$$

where *k* is the intrinsic permeability (L^2); ρ is the density of the fluid (M/L^3); g is gravitational acceleration (L/T^2); and μ is the dynamic viscosity (M/LT); (de Marsily, 1986). Intrinsic permeability is a function of only the natural media, therefore an aquifer will have different hydraulic conductivities for water and LNAPL but the aquifer has the same intrinsic permeability for both fluids. Typical

ranges for hydraulic conductivity and intrinsic permeability are shown in Tables 2.1 and 2.2.

Natural Media

Material	Hydraulic Conductivity (water) (m/s)	Intrinsic Permeability (m^2)
Clay	10^{-11} - 10^{-8}	~10^{-18} - 10^{-15}
Silt, Sandy Silts, Clayey Sands, Till	10^{-8} - 10^{-6}	~10^{-15} - 10^{-13}
Silty Sands, Fine Sands	10^{-7} - 10^{-5}	~10^{-14} - 10^{-12}
Well-sorted Sands, Glacial Outwash	10^{-5} - 10^{-3}	~10^{-12} - 10^{-10}
+Well-sorted Gravel	10^{-4} - 10^{-2}	~10^{-11} - 10^{-9}

Table 2.1: Hydraulic conductivity (water phase) and intrinsic permeability values for unconsolidated sediments (adapted from Fetter, 2001).

Media	Hydraulic Conductivity (m/s)
Dolomitic Limestones	10^{-3} – 10^{-5}
Weathered Chalk	10^{-3} – 10^{-5}
Unweathered Chalk	10^{-6} – 10^{-9}
Limestone	10^{-5} – 10^{-9}
Sandstone	10^{-4} – 10^{-10}
Granite, Gneiss, Basalt	10^{-9} – 10^{-13}

Table 2.2: Hydraulic conductivity values (water phase) for unfractured rocks (de Marsily, 1986).

Borehole Construction

The hydraulic conductivity values for borehole construction were based on the filter pack and annular seal. The fact that the inside of a borehole is an empty space was also considered. These values were used in the numerical model constructed in this study to determine the influence of borehole construction on two-phase flow.

Filter Pack

Filter pack material should consist of clean, well rounded, homogeneous sand or gravel. Using this type of material increases the permeability and porosity of the filter pack. Filter packs are beneficial in highly uniform, fine grained or highly laminated sediments (Driscoll, 1986). The hydraulic conductivity, *K*, of a filter pack is estimated using Equation 2.2. Driscoll (1986) determined upper limit for the hydraulic conductivity of filter pack material to be 17,000 gpd/ft^2 (8.02x10^{-3} m/s).

Annular Seal

An annular seal typically consists of bentonite chips or pellets. Bentonite is composed of smectite minerals which have a low hydraulic conductivity to water, large cation exchange capacity, high swelling potential, and large surface area. The most common bentonite is calcium and sodium bentonite. At a confining stress of 35 kPa, the hydraulic conductivity of calcium bentonite is

$6x10^{-11}$ m/s and sodium bentonite is $6x10^{-12}$ m/s, relative to tap water (Gleason, et al., 1997).

Capillary Pressure and Fluid Saturation

Capillary pressure and saturation of two fluid phases (water and LNAPL) are based on the pore size distribution within the natural media. Capillary pressure is defined as the pressure difference between the non-wetting (LNAPL) and wetting (water) phases in porous media (Charbeneau, 2000). Fluid saturation equals the volume of a fluid divided by the volume of void space. Within a two-phase system the void space within the porous media is assumed to be completely filled with LNAPL and/or water, therefore the fluid saturation of either phase can range from 0 to 1 (Charbeneau et al., 1999).

van Genuchten Model Parameters

The relationship between capillary pressure and saturation is determined by using soil moisture characteristic curves (Figure 2.3). Data for capillary pressure and water content are often measured in laboratory experiments and then fit with mathematical models to produce smooth curves.

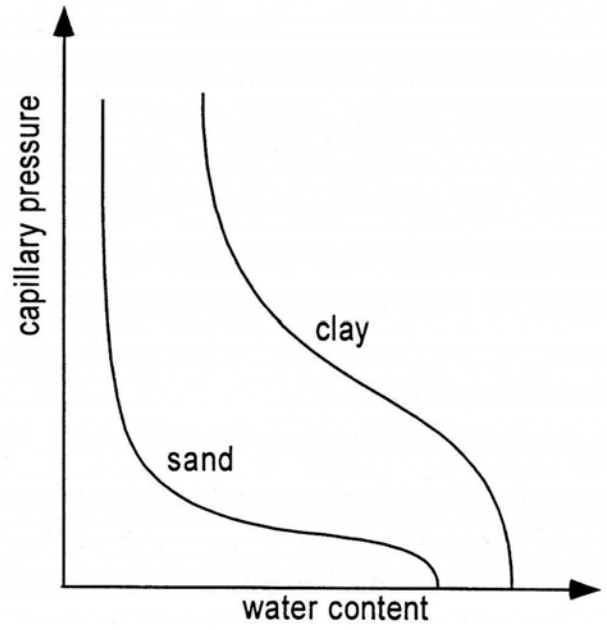

Figure 2.3: Typical soil moisture characteristic curves (Charbeneau et al., 1999).

Brooks and Corey (1964) and van Genuchten (1980) are the two most widely used fitting models (Charbeneau et al., 1999). The model developed in this study uses the van Genuchten (1980) model parameters. Table 2.3 is representative of average van Genuchten parameters for a given soil type.

Soil Type	Saturated Water Content	Residual Water Content	N	α (m^{-1})	α (ft^{-1})	Hydraulic Conductivity (m/s)	Hydraulic Conductivity (ft/d)
Silty-Clay	0.36	0.070	1.09	3.175	0.15	5.64×10^{-8}	0.016
Sand	0.43	0.045	2.68	14.43	4.4	8.11×10^{-5}	23

Table 2.3: van Genuchten parameters (modified from Charbeneau et al., 1999 after Carsell and Parish, 1988). N is the range in the pore sizes. Alpha (α) is proportional to the size of the largest pores in the porous media.

Two-phase Flow and Wells

To the author's knowledge, no previous modeling efforts have been used to determine the type of flow field that is created around a borehole based on the hydraulic conductivity contrast between the borehole and surrounding natural media in a two-phase oil/water system. However, several studies have been conducted to examine the relationship between fluid levels measured in wells and the volume of LNAPL in the surrounding porous media. In the 1980s, the conceptual understanding of LNAPL within a formation was a floating layer of LNAPL on the saturated zone and was referred to as the "pancake" model (Adamski et al., 2007; Figure 2.4).

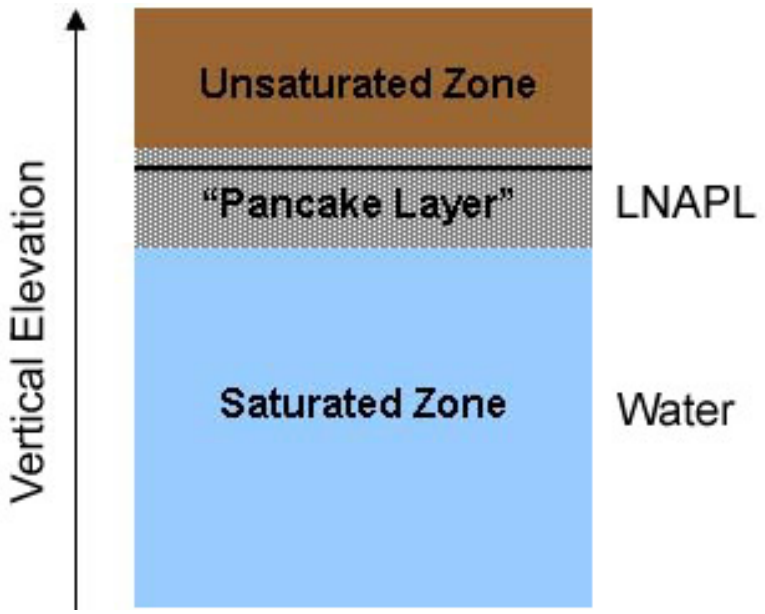

Figure 2.4: "Pancake layer" conceptualization model (modified after Adamski et al., 2007).

Beginning in the 1990's, several studies found that a "pancake" layer of LNAPL does not exist in wells (Charbeneau et al., 1999). Further more, these

studies also showed that the relationship between a well and the surrounding media is more complex than a simple linear correlation. Factors affecting the measurement of LNAPL thickness in a formation include multiphase interaction in the well (Kembloski and Chiang, 1990; Ballestero et al., 1994; Sleep et al., 2000), capillary pressure (Farr et al., 1990; Lenhard and Parker, 1990; Vogler et al., 2001; Aral and Liao, 2002; Huntley et al., 1994a), ground water table fluctuations (Ballestero et al., 1994; Liao and Aral, 1999; Vogler et al., 2001; Aral and Liao, 2002), sediment variability (Wallace and Huntley, 1992; Huntley et al., 1994; Ballestero et al., 1994; Adamski et al., 2005) and sediment pore size (Lenhard and Parker, 1990) in the aquifer.

All of the studies developed either numerical, analytical, or conceptual models based on theoretical, experimental, and field data. Most of the models assume homogenous media and mechanical equilibrium between the well and formation. However, Sleep et al. (2000) found that mechanical equilibrium and homogenous media can not be assumed for accurate volume estimations of the LNAPL. In order for equilibrium conditions to be achieved between a well and the formation, the vertical pressure distributions of the two-phases (water and LNAPL) must be hydrostatic (Figure 2.5; Charbeneau, 2000). Hydrostatic conditions imply there is no lateral or vertical movement of the fluid and the pressure gradient results from the vertical attribute of the overlying fluids (Dahlberg, 1995).

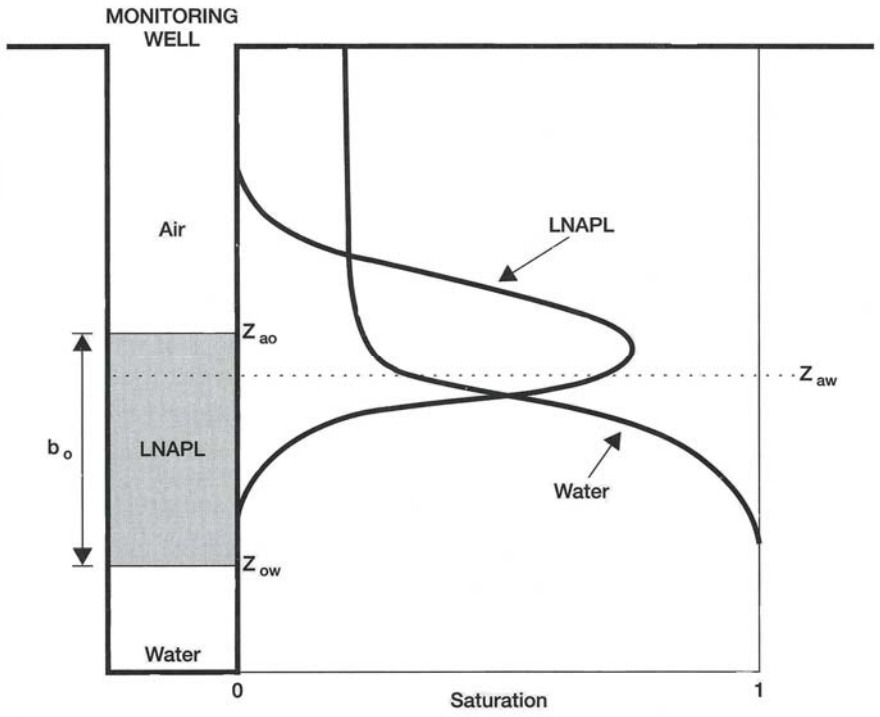

Figure 2.5: Phase distribution under static equilibrium conditions between a well and the natural media (Charbeneau et al., 2000).

Lenhard and Parker (1990) and Farr et al. (1990) both developed analytical models to estimate the actual LNAPL volume in the formation by vertically integrating the LNAPL saturation profile from a monitoring well. Both studies noted that LNAPL does not form “oil-saturated pancakes” or distinct floating layers on the capillary fringe. Lenhard and Parker (1990) concluded that the volume of LNAPL in the subsurface is a function of the LNAPL, water, and air pressure, and distribution of pore-sizes in the porous media. Lenhard (1990) demonstrated how Lenhard and Parker (1990) and Farr et al. (1990) formulated similar equations for estimating the volume of LNAPL in the subsurface from fluid levels in a well, by assuming mechanical equilibrium and homogeneous soils. The models show that different volumes of LNAPL within the subsurface may

produce the same thickness of LNAPL within the monitoring well. The authors concluded that a linear relationship does not exist between the thickness of LNAPL in a monitoring well and the surrounding porous media. Farr et al. (1990) also found that the volume of LNAPL in a formation is highly dependent upon capillary properties of the porous media.

Kembloski and Chiang (1990) examined factors that control fluctuations in hydrocarbon thicknesses measured in monitoring wells. Both equilibrium and non-equilibrium conditions were analyzed and compared to field data. Equilibrium conditions assume that the vertical pressure head gradient is negligible and the net flow of fluids is zero between the well and surrounding porous media. A negative correlation was observed between the measured hydrocarbon thickness and the change of hydrocarbon/water interface elevation under non-equilibrium conditions. This inverse relationship was produced by preferred flow around monitoring wells in conjunction with differing residual hydrocarbon saturations above and below the hydrocarbon/water interface. The authors concluded that the hydrocarbon thickness in porous media can not be determined from monitoring wells. A geophysical approach was recommended to estimate the oil distribution in a formation.

Ballestero et al. (1994) related the apparent thickness of LNAPL in a monitoring well to the actual LNAPL thickness in the formation. The authors found that the main factors in determining the actual LNAPL thickness include apparent product thickness in the well, product density, water table fluctuations,

and grain size distribution in the aquifer. The authors formulated an equation to predict the thickness of gasoline in a uniform sand aquifer as follows:

$$t_g = t(1 - S_g) - h_a \tag{2.3}$$

where t_g is the actual hydrocarbon thickness, t is the apparent thickness, S_g is the specific gravity of the hydrocarbon, and h_a is the distance between hydrocarbon and the water table. Note that water table fluctuations were not considered in this equation.

Huntley et al. (1994b) investigated the influence of sediment variability on volume estimations of hydrocarbons. The study was conducted at two sites with relatively homogenous fine grained sandstone aquifers. A similar study was conducted by Wallace and Huntley (1992). Soil saturation/ capillary pressure characteristic curves were plotted from aquifer grain size data. Both studies found that a single "average" soil sample is not representative of an aquifer and can not be used to calculate the actual amount of hydrocarbon, even on small sites. Grain-size distribution data was even found to produce errors in the volume estimation of hydrocarbon. Both papers concluded that the apparent hydrocarbon thickness measured in a monitoring well should be corrected with soil saturation/capillary pressure characteristic curves to more accurately estimate the hydrocarbon volume. Hydrocarbon volumes were calculated using the Van Genuchten fitting parameters (α, n, and residual saturation) and the corresponding curve.

Beckett and Huntley (1998) used a three dimensional, finite-element model, MAGNAS3 to study the effect of soil type on LNAPL recovery rates.

Three different soil types were modeled with air, water, and LNAPL phases included. Several recovery designs were simulated to determine which was most effective for each soil. The authors noted that hydrocarbon saturation and movement within the subsurface was dependent on fluid properties, soil capillarity, and permeability. The study concluded that recovery efforts in any type of soil decreased the permeability around the well which decreased the LNAPL saturation and mobility into the well.

Liao and Aral (1999) used two analytical models to examine the effect of unsteady ground water fluctuations on the amount of LNAPL in a monitoring well. The models simulated an unconfined aquifer with rising and falling piezometric head conditions. Residual saturation of the LNAPL was assumed to be constant. The models indicated that ground water fluctuation has a significant effect on LNAPL measurements which would cause error in volume calculations of LNAPL in the porous media. The authors concluded that their models represented a method to estimate hydraulic equilibrium conditions at contaminated sites.

Sleep et al. (2000) developed a numerical model to determine LNAPL thickness in finite volume monitoring wells. The model incorporated gravity segregation of water, air, and LNAPL for multiphase flow. A pilot scale experiment which consisted of layered sandy soil and toluene injection was conducted to test the validity of the model. Results from the experiment and model indicated mechanical equilibrium and soil homogeneity could not be assumed in order to accurately determine the volume of LNAPL within the soil.

Vogler et al. (2001) developed an empirical method to estimate the volume of hydrocarbon contamination within the subsurface from fluid levels in monitoring wells. This method calculated the LNAPL volume by using the oil-air, water-air, and oil-water capillary pressure and saturation relationships. The authors noted that the capillary properties of porous media significantly impact multiphase flow. A laboratory experiment and field investigation was conducted to study the influence of ground water table fluctuations on flow. The authors concluded that in order to determine the actual volume of LNAPL contamination their method and ground water table fluctuations must be considered.

Aral and Liao (2002) used a numerical model to investigate the impact of water table and capillary pressure fluctuations on LNAPL thickness in monitoring wells. The authors found that under transient conditions, LNAPL thickness in the monitoring well were not reflective of the total volume of contamination in the formation. Capillary pressure at the LNAPL/air and water/LNAPL interfaces significantly affected the thickness of LNAPL in the monitoring well.

Adamski et al. (2005) developed a conceptual model for LNAPL behavior in fine grained soil. The authors found that in fine grained soils, macropores controlled the distribution of LNAPL in the formation. They also concluded that LNAPL saturation in fine grained soil could be predicted by using the Charbeneau/API model (Charbeneau et al., 1999), site hydrogeology, soil sampling, and saturation properties of the soil.

A linear relationship does not exist between the porous media and LNAPL thickness within a well. Many studies have concluded that mechanical

equilibrium between the well and media can not be assumed due to temporal fluctuations in the water table and capillary pressures; sediment and pore size variability; and multiphase interaction in the well. For these reasons monitoring wells should not be utilized as the only tool at sites contaminated by LNAPL to determine the extent of contamination within the subsurface. Additionally, a well which does not present detectable levels of hydrocarbon should not be used to determine if a LNAPL contaminated site is “clean”.

Electrical Resistivity Imaging

Electrical resistivity imaging has progressively become a useful and sophisticated method to map the extent of LNAPL contamination (Halihan et al., 2005a). Electrical resistivity measurements are collected through a series of electrodes which emit current into the subsurface. The potential field is recorded and the data is inverted to create a map of subsurface resistivity distributions. ERI is the general term used to describe an array of electrodes on the surface, without naming each electrode configuration. In contrast, electrical resistivity tomography (ERT) indicates the electrodes are in the subsurface measuring the electrical conductivity of the ground (Halihan et al. 2005c).

Daily et al. (1995) conducted three controlled experiments to assess the accuracy of ERT for the characterization and monitoring of hydrocarbon contaminated sites. The experiments were performed in a tank which was 10 m^2 and 5 m deep. The experiments included a gasoline spill into a sandy soil, air sparging in a saturated soil, and a leaky oil storage tank. All of the experiments

produced resistive anomalies in the ERT images in both saturated and unsaturated sediment. LNAPL was confirmed through coring to be in the location of the resistive anomalies.

Benson and Mustoe (1996) determined the extent of hydrocarbon contamination from a leaky underground storage tank using electrical resistivity and ground penetrating radar (GPR). GPR data and isoresistivity maps constructed from the resistivity surveys were used to select locations for monitoring wells. The authors concluded that geophysical surveys are a cost effective method to collect data and reduces the risk of blind drilling into hazardous waste materials.

Loh et al. (1999) investigated the use of ERT to calculate volumetric flow rates of conductive liquids in nonconductive solids. The authors compared flow rates derived from ERT to those derived from more traditional methods such as weighing hoppers, gradiomanometers, and intrusive conductivity probes. There was a good correlation between the results, indicating that ERT can be used to determine flow rates.

Atekwana et al. (2000) employed multiple geoelectrical methods and soil borings to analyze a 50-year-old hydrocarbon contaminated site. Geoelectrical methods included ground penetrating radar (GPR), electrical resistivity (both surface and downhole), and electromagnetic induction. The objective was to determine if the temporal variation in the electrical signal of the LNAPL from resistive to conductive. The authors found that the electrical signal of the hydrocarbon did change and hypothesized that this was a result of LNAPL

biodegradation. Therefore, the assumption that LNAPL always produces regions of high resistivity above the water table in geophysical images is not always correct, due to the evolving nature of the plume. The authors concluded that surface and downhole geoelectrical measurements at LNAPL contaminated sites allow for a better site characterization as compared to using only monitoring wells to delineate LNAPL within the subsurface.

Delaney et al. (2001) examined the change in resistivity of fine-grained soils at a petroleum contaminated site with both laboratory and field investigations. The authors noted that electrical resistivity values for clean soils range from 100 to 10,000 ohm-meters, while unsaturated coarse grained and frozen soils typically exceed 10,000 ohm-meters. The field survey and laboratory experiments showed that a soil will have a permanent increase in resistivity due to residual hydrocarbon contamination. The authors concluded that at petroleum contaminated sites resistivity values are site dependent.

Kemna et al. (2002) used ERT to image a field tracer (NaBr) experiment in a heterogeneous unconfined aquifer. The authors noted that it is difficult for monitoring wells to depict the complex position and shape of a plume. ERT images taken during the experiment were converted to solute concentration maps and depicted the spreading of the plume over time. The authors found this method to be more valuable than using monitoring wells since it allows for the determination of the center of the plume and has better resolution.

Halihan et al. (2005a) applied ERI to locate remaining hydrocarbons in an already remediated site. ERI images detected “blobs” of hydrocarbons remaining

inside and outside of the remediated area. Hydrocarbons were also detected in between “clean” monitoring wells. The images were confirmed with drilling. The authors concluded that ERI is a more efficient and cost effective method to locate hydrocarbon contamination than installing numerous monitoring wells at the site.

COMSOL Multiphysics

This finite element modeling program allows for the simulation of any physical phenomenon that can be expressed as a set of partial differential equations. The program is capable of using multiple equations in a single model. Grechka and Soutter (2005) used COMSOL to model two-phase flow (oil and water) fully coupled to the deformation that occurs during fluid production and injection within a porous reservoir. The model was governed by the equations established by Brooks and Corey (1966), van Genuchten (1980), and Thurston (1974). This simulation incorporated changes in pressure, saturation, flow velocity, and permeability for both oil and water phases.

CHAPTER III

METHODOLOGY

A numerical model was developed to determine the influence of borehole construction on LNAPL thickness measurements. This was be done by modeling the hydraulic conductivity contrast between the borehole and media to determine if the two-phase (water and LNAPL) flow field around a borehole is significantly affected. This chapter presents the two-phase flow numerical simulation by first defining the model geometry, then establishing the governing equations and constitutive relationships that define fluid retention and permeability in the natural media. The formulation of boundary conditions and initial conditions follows.

Numerical Model Development

The two-phase flow numerical simulation was constructed using COMSOL Multiphysics 3.3a. The numerical model was created in the Earth Science Module. This module allowed for the simulation of numerous geophysical and environmental scenarios.

Model Geometry

Two-phase flow in the model was driven by a lateral gradient which allowed the water and LNAPL to flow horizontally into one side of the aquifer and

out the other (Figure 3.1). The dimensions of the aquifer were 50x50 m, with a borehole in the center. The radius of the borehole was varied in certain simulations to examine the influence of borehole size on the two-phase flow field.

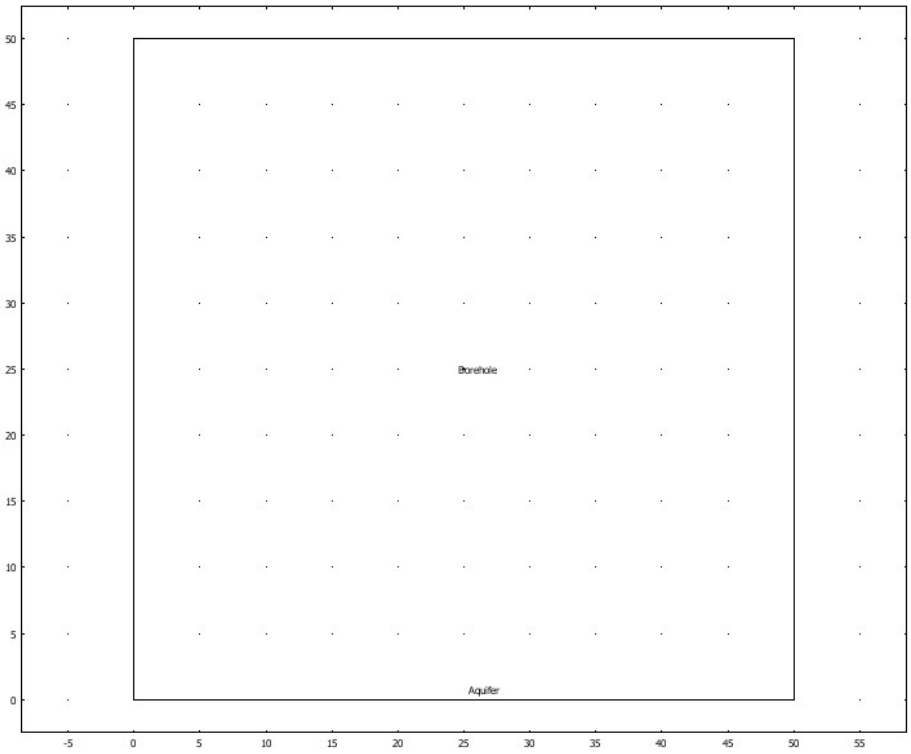

Figure 3.1: Model geometry in plan view. Scale is in meters.

The domains of the model geometry were subdivided into triangles or elements which make up the mesh (Figure 3.2). A normal mesh was generated for the natural media and a finer mesh was applied to area near the borehole to better define the physics occurring in this area.

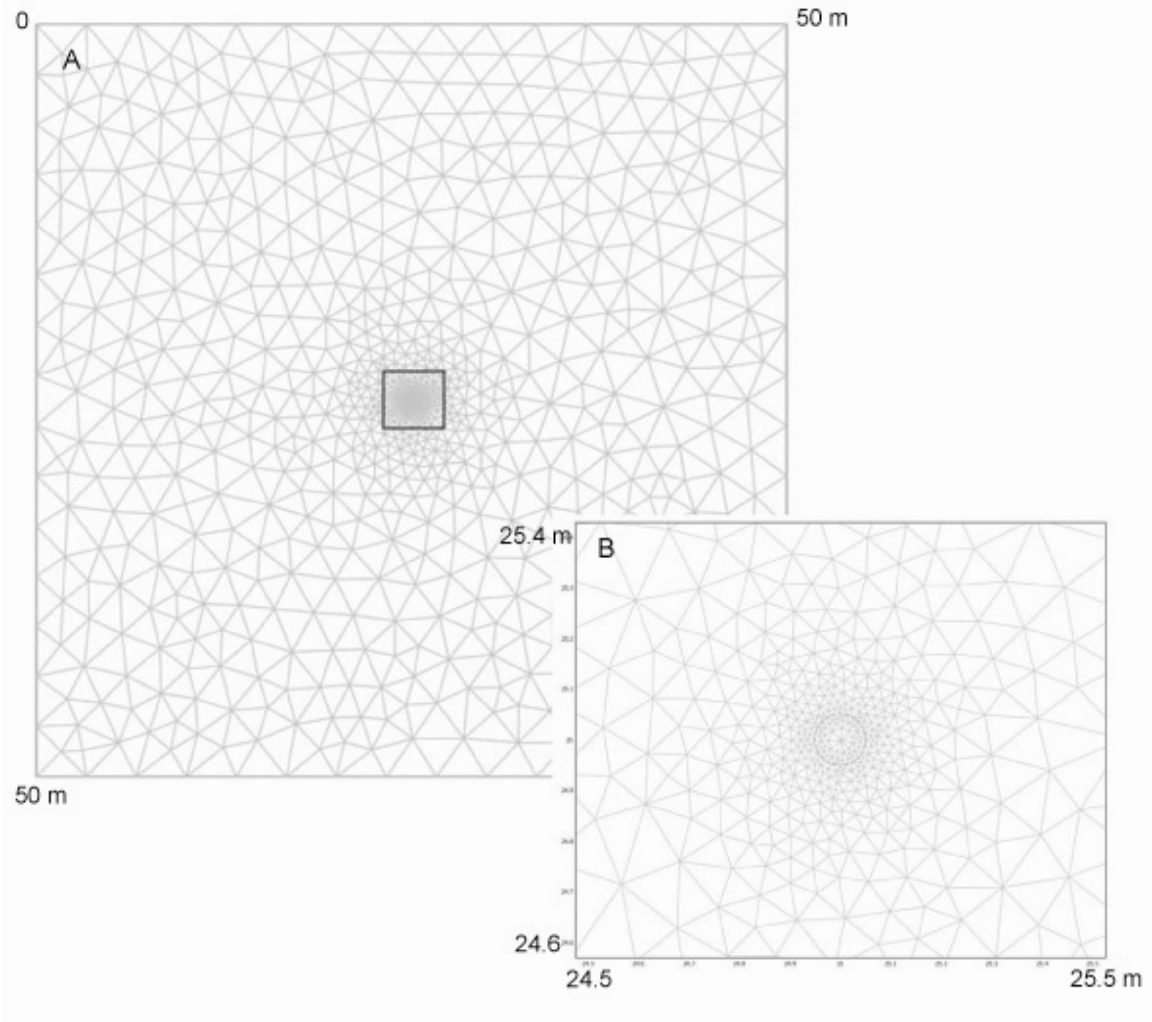

Figure 3.2: Mesh of model. A.) Mesh of the whole aquifer and B.) area closest to the borehole. The scale is in meters for both figures.

Governing Equations and Constitutive Relationships

The governing equations for two-phase flow in porous media follow separate mass conservation equations for the wetting and non-wetting fluids. Water is considered to be the wetting fluid since water favors contact with the solid matrix (i.e. mineral grains making up the aquifer). LNAPL is the non-wetting fluid which means it has a lower tendency to interact with the solid matrix as compared to water (Charbeneau, 2000).

The governing equations for multiphase flow are coupled, nonlinear partial differential equations (PDEs). Constitutive relationships are also integrated into the PDEs to account for fluid retention and aquifer permeability. The governing equations and constitutive relationships were taken from a two-phase flow example in the COMSOL Multiphysics Earth Science Module (2005). The following equations are based on Mualem (1976) and van Genuchten (1980).

The mass conservation equations for the wetting (*w*) and non-wetting (*nw*) fluids, assuming they are incompressible, are:

$$\theta_s \frac{\partial Se_w}{\partial t} + \nabla \cdot \left[-\frac{\kappa_{\text{int}} k_{r,w}}{\eta_w} \nabla \left(p_w + \rho_w g D \right) \right] = 0 \tag{3.1}$$

$$\theta_s \frac{\partial Se_{nw}}{\partial t} + \nabla \cdot \left[-\frac{\kappa_{\text{int}} k_{r,nw}}{\eta_{nw}} \nabla \left(p_{nw} + \rho_{nw} g D \right) \right] = 0 . \tag{3.2}$$

See the List of Symbols section for nomenclature descriptions. Equations 3.1 and 3.2 are subject to the constraint:

$$Se_w + Se_{nw} = 1. \tag{3.3}$$

This constraint assumes that the void space of the porous media is completely filled by water and/or LNAPL. The saturation of either fluid phase can range from 0 to 1.

Capillary pressure is the pressure difference between the non-wetting and wetting phase interfaces and is mathematically defined as:

$$p_c = p_{nw} - p_w. \tag{3.4}$$

Capillary pressure results from the density difference between two fluids and is a function of the fluid phase saturations. Effective saturation changes with capillary pressure. This relationship is quantified as:

$$C_{p,w} = -C_{p,nw} = \theta_s \frac{\partial Se_w}{\partial p_c} \tag{3.5}$$

where C_p is the specific capacity of the wetting and non-wetting phases at a given pressure.

To numerically simplify the model, Equations 3.3, 3.4, and 3.5 are substituted in Equations 3.1 and 3.2, so that the governing equations become:

$$C_{p,w} \frac{\partial}{\partial t}\left(p_{nw} - p_w\right) + \nabla \cdot \left[-\frac{\kappa_{\text{int}} k_{r,w}}{\eta_w} \nabla\left(p_w + \rho_w g D\right) \right] = 0 \tag{3.6}$$

$$-C_{p,w} \frac{\partial}{\partial t}\left(p_{nw} - p_w\right) + \nabla \cdot \left[-\frac{\kappa_{\text{int}} k_{r,nw}}{\eta_{nw}} \nabla\left(p_{nw} + \rho_{nw} g D\right) \right] = 0 . \tag{3.7}$$

Fluid Retention and Permeability

The van Genuchten (1980) and Mualem (1976) equations are dependent on capillary pressure head (H_c) to express fluid retention and permeability for two-phase flow. The following relationships define how θ, S_e, C, k_r, and p_c vary simultaneously by transforming capillary pressure to capillary pressure head which is defined as:

$$H_c = \frac{p_c}{\rho_w g} . \tag{3.8}$$

The hydraulic properties of the wetting fluid phase are given by Equations 3.9-3.12, with the variables defined in the List of Symbols:

$$\theta_w = \begin{cases} \theta_{r,w} + Se_w(\theta_{s,w} - \theta_{r,w}) & H_c > 0 \\ \theta_{s,w} & H_c \le 0 \end{cases} \tag{3.9}$$

$$Se_w = \begin{cases} \dfrac{1}{\left[1 + \left|\alpha H_c\right|^n\right]^m} & H_c > 0 \\ 1 & H_c \le 0 \end{cases} \tag{3.10}$$

$$C_w = \begin{cases} \left(\dfrac{\alpha m}{1-m}\theta_{s,w} - \theta_{r,w}\right) Se_w^{\frac{1}{m}} \left(1 - Se_w^{\frac{1}{m}}\right)^m & H_c > 0 \\ 0 & H_c \le 0 \end{cases} \tag{3.11}$$

$$k_{r,w} = \begin{cases} Se_w^{\,L}\left[1 - \left(1 - Se_w^{\frac{1}{m}}\right)^m\right]^2 & H_c > 0 \\ 1 & H_c \le 0 \end{cases} \tag{3.12}$$

The hydraulic properties of the non-wetting fluid are given by Equations 3.13-3.16:

$$\theta_{nw} = \theta_{s,w} - \theta_w \tag{3.13}$$

$$Se_{nw} = 1 - Se_w \tag{3.14}$$

$$C_{nw} = -C_w \tag{3.15}$$

$$k_{r,nw} = \left(1 - Se_w\right)^L \left(1 - Se_w^{\frac{1}{m}}\right)^{m^2} \tag{3.16}$$

Boundary and Initial Conditions

The boundary conditions in the model for both phases were either hydrostatic or no-flow. These conditions simulated a confined aquifer and only allowed the water and LNAPL to flow laterally from one side to the other (Figure 3.3).

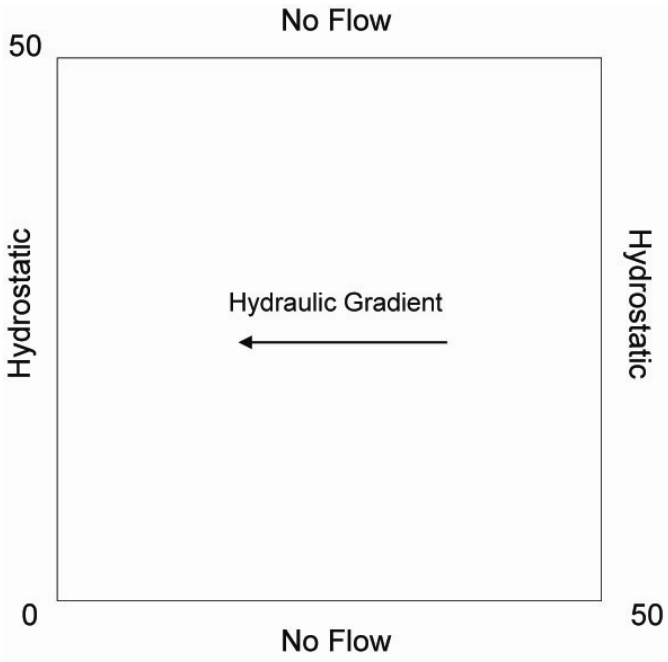

Figure 3.3: Boundary conditions for the model aquifer shown in plan view. Scale is in meters.

The boundary condition and initial conditions were expressed in terms of pressure:

$$p = \rho g h \ . \tag{3.17}$$

For the wetting phase, the boundary condition on the right side of the aquifer was set at 509 Pascals (1 Pa= 1 kg/ms^2) and the left is 18 Pa. Initial conditions for the wetting phase were set as:

$$p(w) = 9.82\,x + 18\,. \tag{3.18}$$

This equated to a hydraulic gradient of 0.001 m/m, where x was the distance along the aquifer which was 50 m long, approximating an ambient gradient an aquifer.

The boundary condition for the non-wetting phase on the right side was a function of pressure and allowed the pressure head to change with time. The

pressure head was set to increase after the initial conditions had reached equilibrium. LNAPL was then introduced into the aquifer and flowed down gradient until a steady state condition was reached between the media and borehole. The pressure head for the LNAPL then returned to the initial head condition which forced the non-wetting phase to leave the system. The left side of the model for the non-wetting phase was set at a constant 983 Pa. For the non-wetting phase, initial conditions were formulated as:

$$p(nw) = 1.1x + 1100\,. \tag{3.19}$$

The head for the non-wetting phase was offset from the head of the wetting phase to account for the density difference between LNAPL (800 kg m^{-3}) and water (1000 kg m^{-3}; Charbeneau, 2000). Hydrocarbon density can range from 780 kg m^{-3} to 900 kg m^{-3} but most commonly occurs in the 800 – 900 kg m^{-3} (Dahlberg, 1995). The boundary condition for the wetting phase resulted in constant pressure conditions on the boundaries for both phases, but variable saturations in the models depended on which was parameter was used (Table 3.1).

Hydraulic Conductivity (m/s)	Intrinsic Permeability (m^2)	Porosity	Residual Porosity	Alpha (m^{-1})	N
10^{-3}	10^{-10}	0.43	0.045	21.78	3.33
10^{-4}	10^{-11}	0.43	0.045	14.44	2.68
10^{-6}	10^{-13}	0.39	0.1	5.91	1.48
10^{-9}	10^{-16}	0.36	0.07	0.49	1.09

Table 3.1: Parameters used in numerical model (compiled by Charbeneau et al., 1999 who adapted them from Carsell and Parish, 1988). Alpha (α) is proportional to the size of the largest pores in the porous media. N is the range in the pore sizes.

CHAPTER IV

RESULTS

The hydraulic conductivity contrast between a borehole and the natural media was modeled to determine if the flow field in an aquifer is affected by this contrast. The contrast was examined by changing the hydraulic conductivity of the borehole to values of 10^{-3} and 10^{-9} m/s, which represented end member cases for well construction. The hydraulic conductivity of the porous media was examined at 10^{-4} and 10^{-6} m/s. The intrinsic permeability, porosity, residual porosity, and van Genuchten parameters were also changed for each simulation to fit the hydraulic conductivity value (Table 3.1).

Convergent Flow Field

A convergent flow field into the borehole was created when the hydraulic conductivity of the borehole is greater than that of the surrounding media (Figure 4.1). A hydraulic conductivity of 10^{-3} m/s was assigned to the borehole to simulate a well surrounded by a sand filter pack. This may be too low for some well construction configurations, but is an order of magnitude above the highest simulated aquifer material. At higher levels, van Genuchten parameters are not well defined for the simulations. A hydraulic conductivity of 10^{-4} m/s for the media represented homogeneous sandstone or unconsolidated sands and

gravels. A silty, clayey sand aquifer was examined by using a hydraulic conductivity of 10^{-6} m/s. The diameter of the borehole in the following simulations is four inches (10.2 cm).

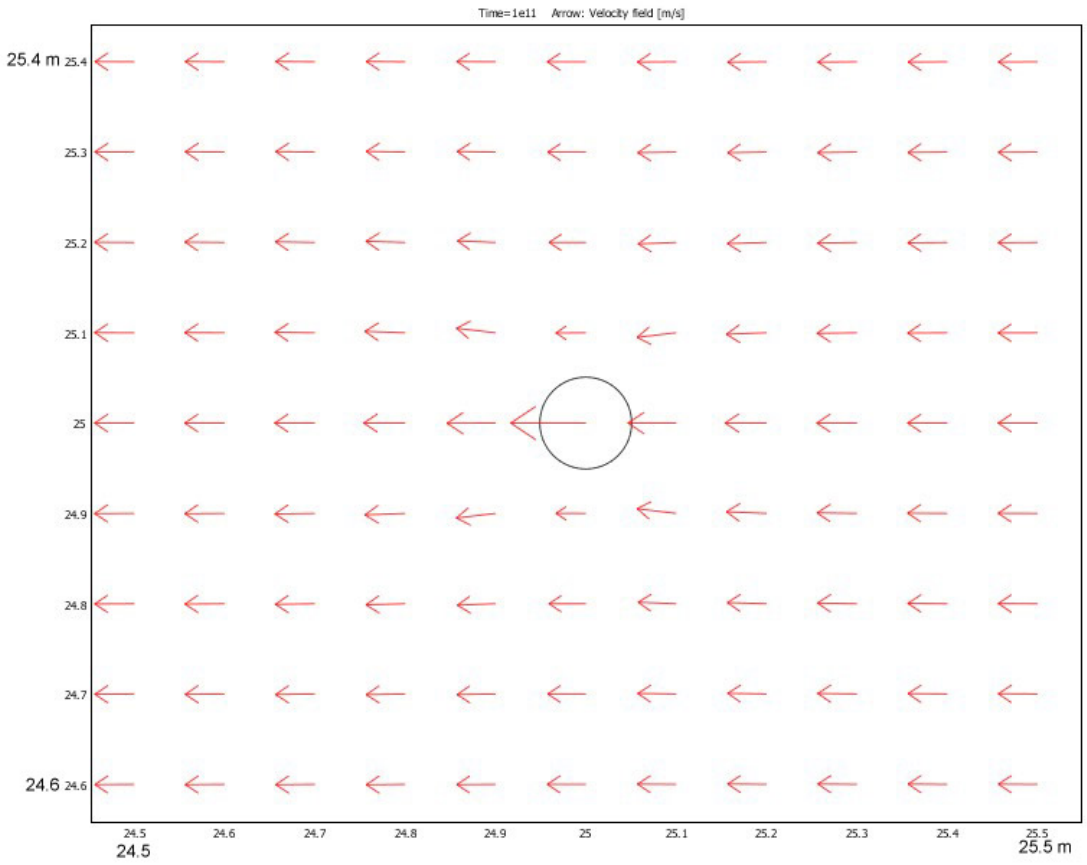

Figure 4.1: Convergent flow field. The scale is in meters.

Sand Aquifer

The saturation of LNAPL within the center of the borehole (Figure 4.2; x=25, y=25) is higher than the saturation outside of the borehole (Figure 4.3; x=25, y=26). When the hydraulic conductivity is greater in the borehole (10^{-3} m/s) than that of the surrounding media (10^{-4} m/s), as seen in Figure 4.2 and 4.3, the preferential flow of the LNAPL is into the borehole. The convergent flow field

causes the LNAPL saturation within the borehole to be greater than the surrounding media, but largely due to hydrostatic effects. The area being influenced by the convergent flow field, also known as the capture zone, extends approximately 0.5 m outward from the center of the well (Figure 4.1).

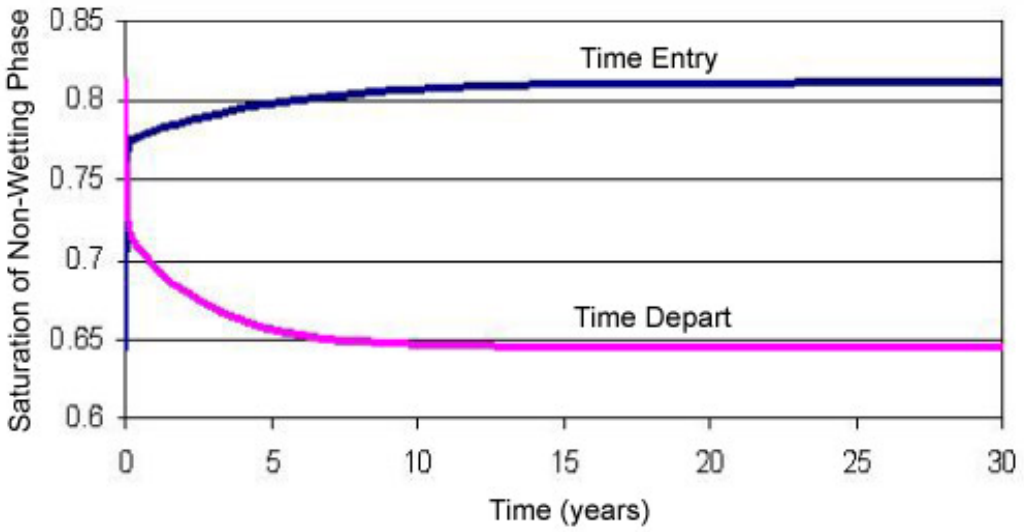

Figure 4.2: Saturation of the non-wetting phase at the center of the borehole (Borehole: K =10^{-3} m/s; Media: K=10^{-4} m/s).

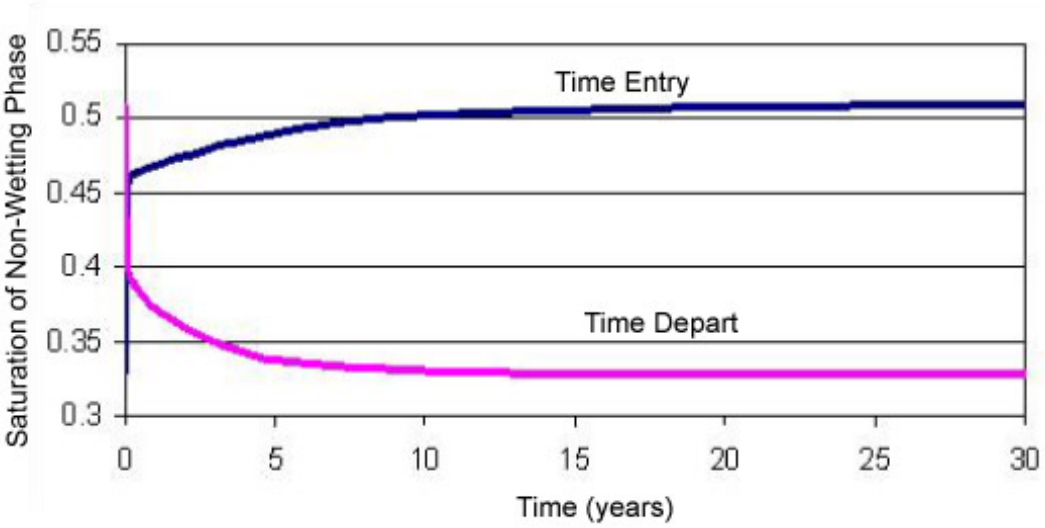

Figure 4.3: Saturation of the non-wetting phase outside of the borehole (Borehole: K =10^{-3} m/s; Media: K=10^{-4} m/s).

When the non-wetting phase enters the borehole the LNAPL reaches equilibrium between the well and surrounding porous media in approximately 21 years (Figure 4.2). As LNAPL departs the borehole equilibrium is once again reached after 13 years. A similar pattern is seen outside of the borehole (Figure 4.3).

Silty, Clayey Sand Aquifer

A convergent flow field remains when the hydraulic conductivity of the aquifer is changed from 10^{-4} m/s to 10^{-6} m/s as seen in higher saturations in the well compared to surrounding media. The amount of LNAPL saturation in the borehole is similar in both aquifers (Figure 4.2 and 4.4). However, the LNAPL saturation outside of the borehole is greater in the sand aquifer (Figure 4.3) as compared to the silty clayey sand aquifer (Figure 4.5). Lower LNAPL saturation in the silty, clayey sand aquifer can be attributed to the lower hydraulic conductivity and the change in van Genuchten parameters. LNAPL reaches equilibrium between the borehole and the silty, clayey sand aquifer in approximately 90 years (Figure 4.4), almost five times longer than in the sand aquifer.

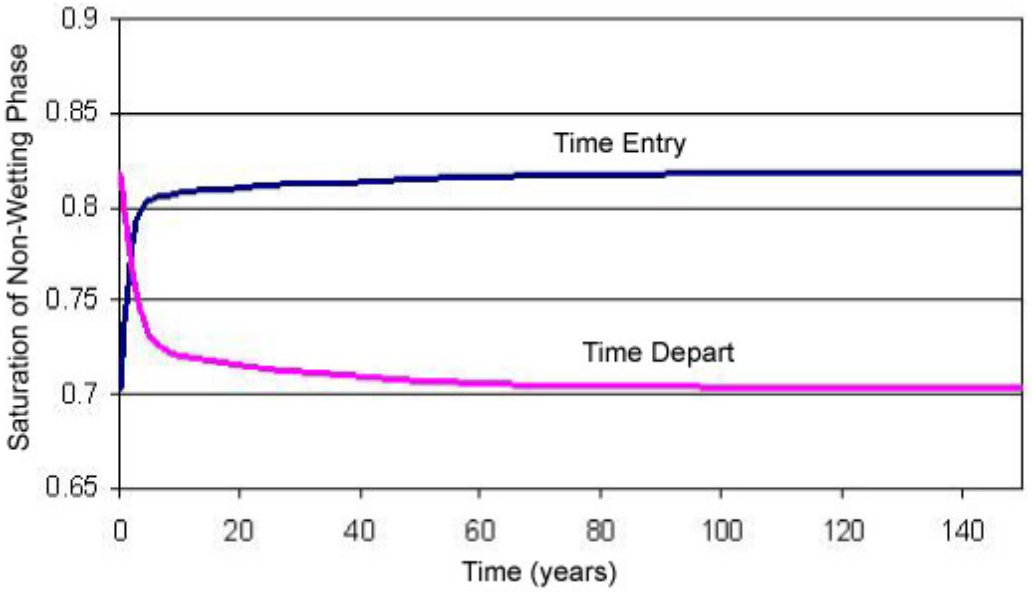

Figure 4.4: Saturation of the non-wetting phase at the center of the borehole (Borehole: K =10^{-3} m/s; Media: K=10^{-6} m/s).

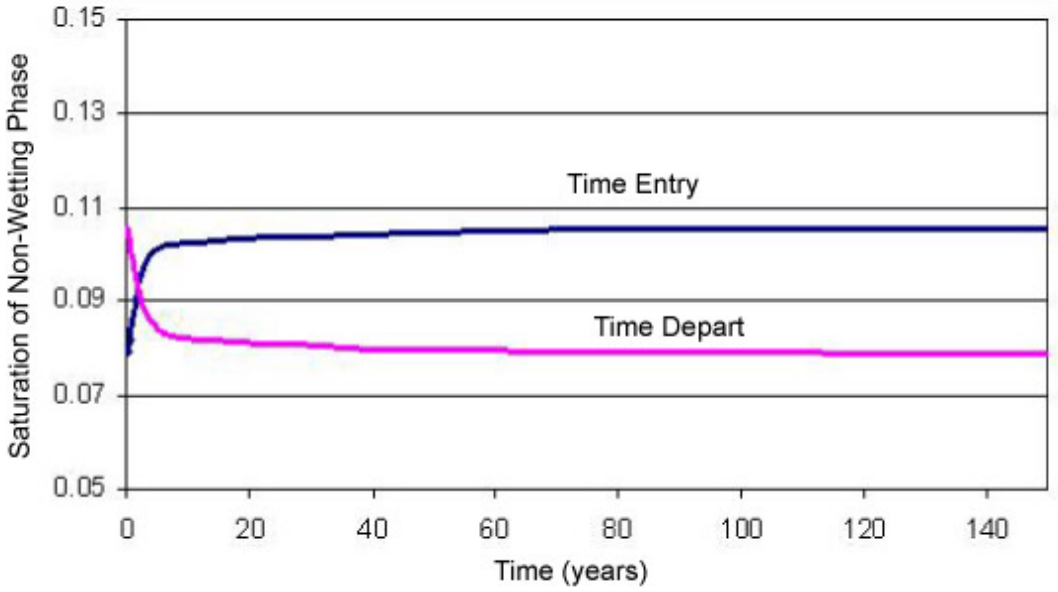

Figure 4.5: Saturation of the non-wetting phase outside of the borehole (Borehole: K =10^{-3} m/s; Media: K=10^{-6} m/s).

Divergent Flow Field

A divergent flow field is created around a borehole when the hydraulic conductivity of the borehole is less than the surrounding media (Figure 4.6). A

hydraulic conductivity of 10^{-9} m/s was applied to the borehole to simulate a sealed boring or installed ERT cable. The hydraulic conductivity of the surrounding porous media was initially set at 10^{-4} m/s to model sandstone or unconsolidated sands and gravels. A silty, clayey sand aquifer was also examined by using a hydraulic conductivity of 10^{-6} m/s. The diameter of the borehole in the following simulation was four inches (10.2 cm).

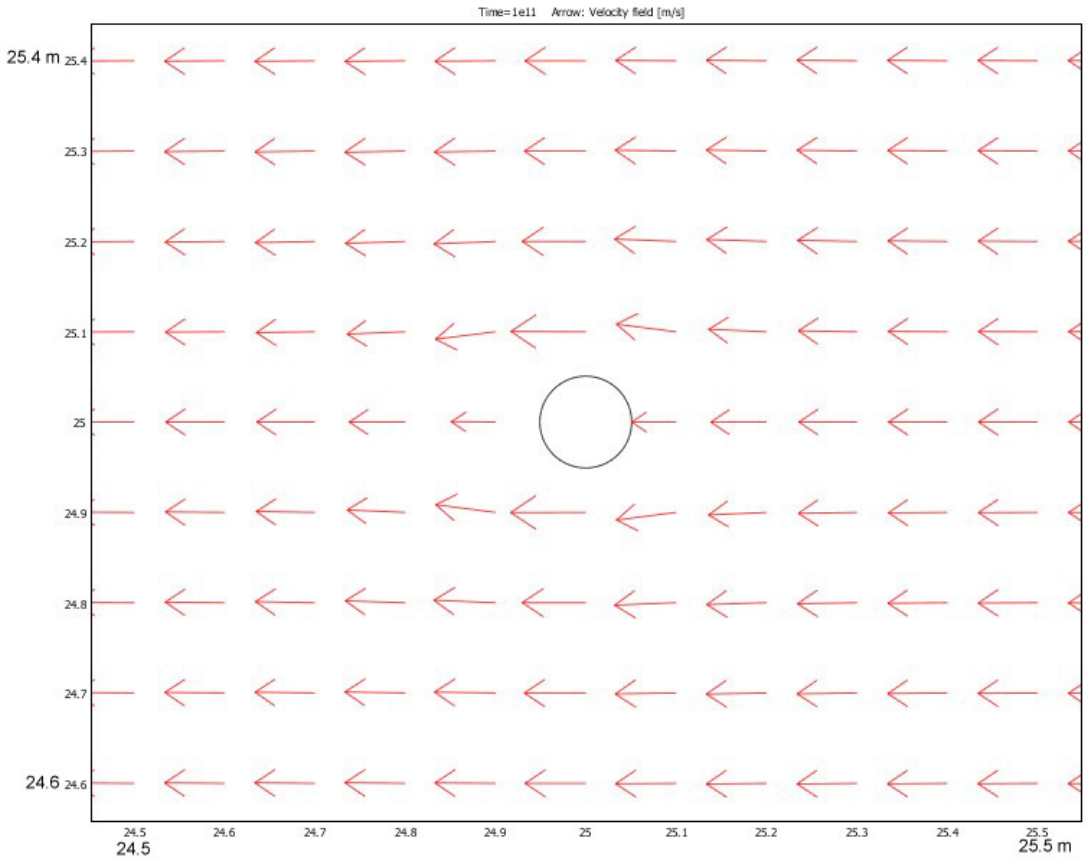

Figure 4.6: Divergent flow field. The scale is in meters.

Sand Aquifer

The saturation of LNAPL within the center of the borehole (Figure 4.7; x=25, y=25) is less than the saturation outside of the borehole (Figure 4.8; x=25,

y=26). When the hydraulic conductivity in the borehole (10^{-9} m/s) is less than media (10^{-4} m/s), as seen in Figure 4.7 and 4.8, the preferential flow of the LNAPL is diverted around the borehole. This divergent flow field causes the LNAPL saturation to be greater within the surrounding media than in the borehole:0.0027 and 0.51, respectively (Figure 4.7 and 4.8). The area influenced by the divergent flow field is approximately 0.5 m from the center of the well.

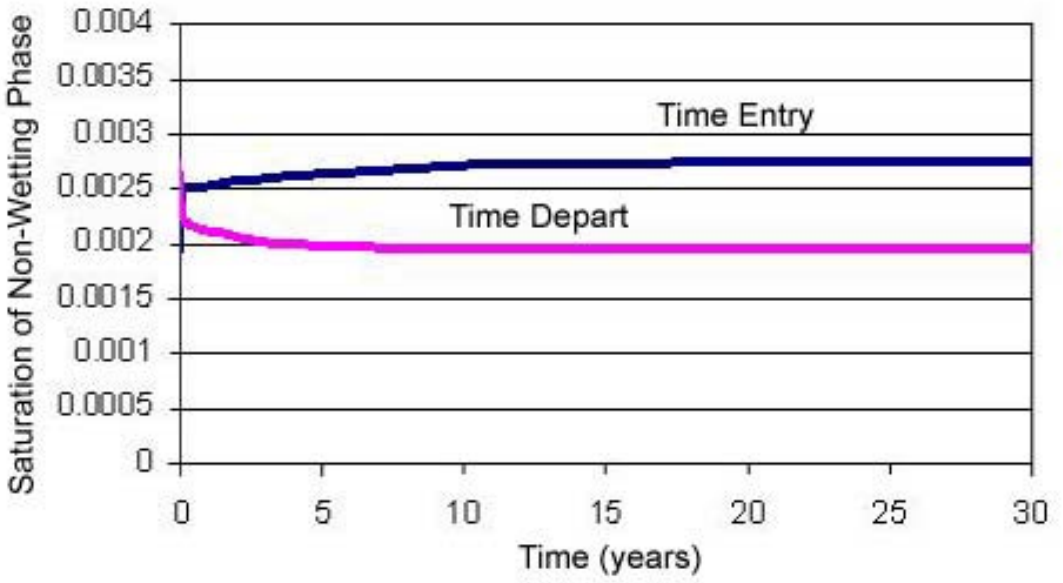

Figure 4.7: Saturation of the non-wetting phase in the center of the borehole (Borehole: K =10^{-9} m/s; Media: K=10^{-4} m/s).

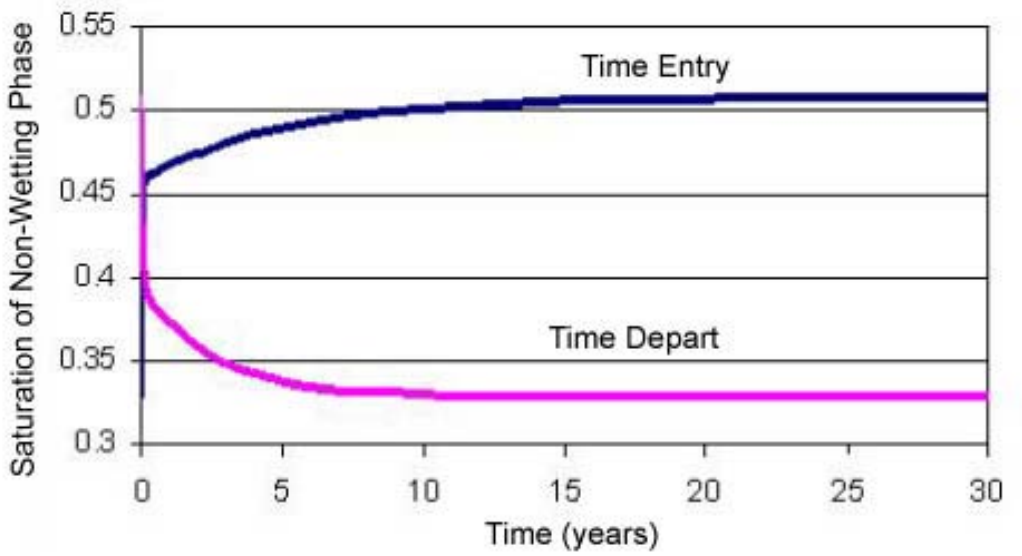

Figure 4.8: Saturation of the non-wetting phase outside of the borehole (Borehole: K =10^{-9} m/s; Media: K=10^{-4} m/s).

When the non-wetting phase enters the borehole the LNAPL reaches equilibrium between the well and surrounding porous media in approximately 20 years (Figure 4.7). As LNAPL departs the borehole equilibrium is once again reached after 9 years.

Silty, Clayey Sand Aquifer

A divergent flow field remains when the hydraulic conductivity of the aquifer is changed from 10^{-4} m/s to 10^{-6} m/s. The LNAPL saturation in the center of the borehole is similar in both aquifers (Figure 4.7 and 4.9). However, the LNAPL saturation outside of the borehole is greater in the sand aquifer than in the silty, clayey sand aquifer: 0.51 and 0.10, respectively (Figure 4.8 and 4.10). Lower LNAPL saturation in the silty, clayey sand aquifer can be attributed to the lower hydraulic conductivity. Almost 100 years is required for the LNAPL to

reach equilibrium between the borehole and silty, clayey sand aquifer (Figure 4.9), as compared to 20 years in the sand aquifer.

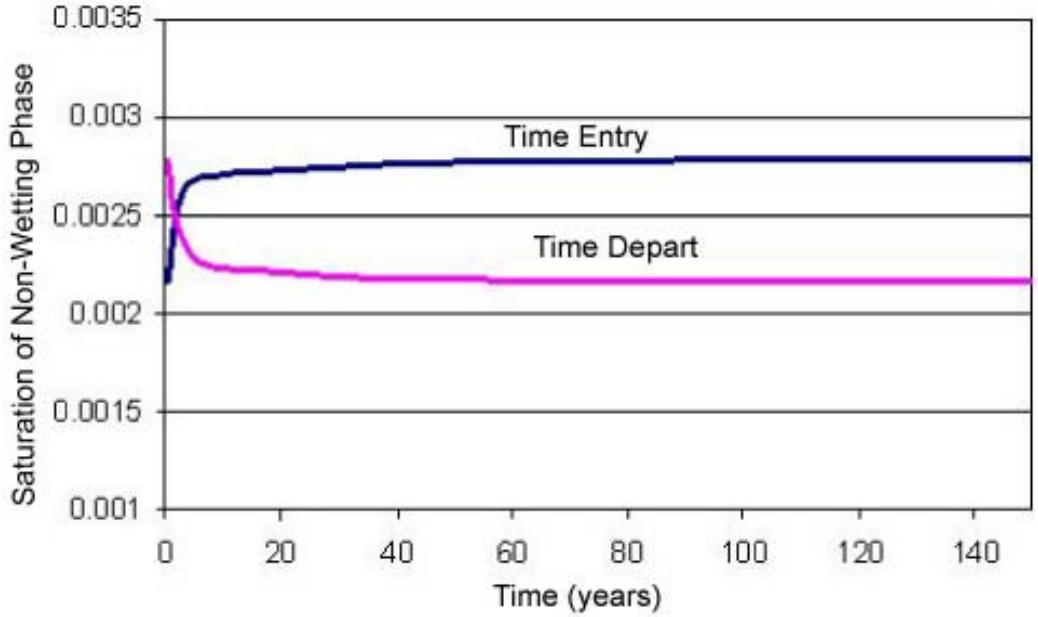

Figure 4.9: Saturation of the non-wetting phase at the center of the borehole (Borehole: K =10^{-9} m/s; Media: K=10^{-6} m/s).

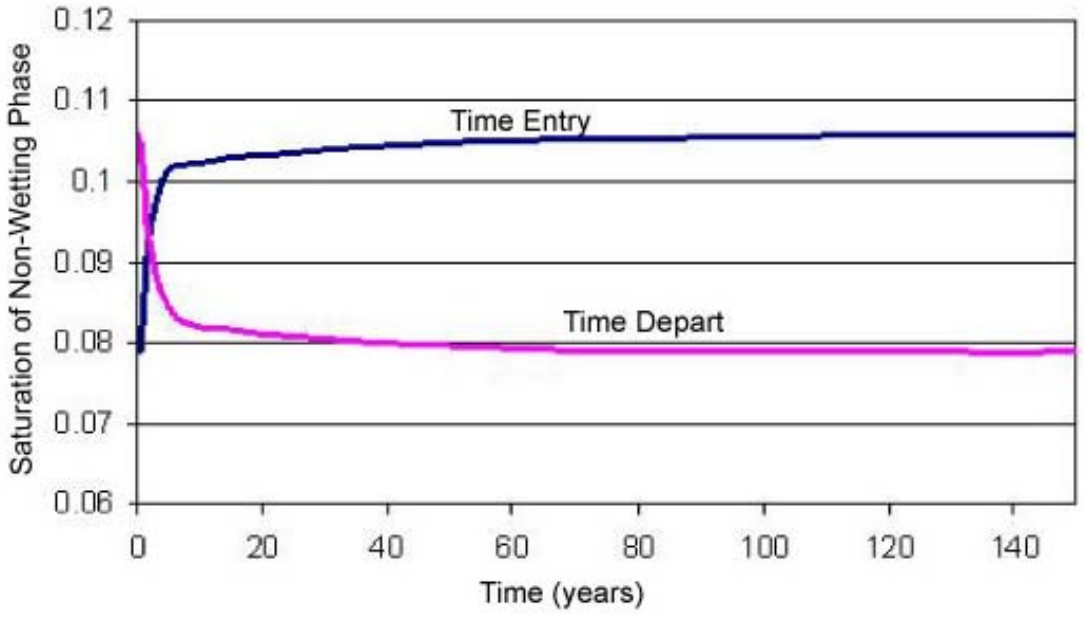

Figure 4.10: Saturation of the non-wetting phase outside of the borehole (Borehole: K =10^{-9} m/s; Media: K=10^{-6} m/s).

Borehole Size

The borehole was decreased to a diameter of 2 inches and increased to 12 inches to determine the effect of borehole size on the LNAPL saturation. The hydraulic conductivity of the natural media was set at 10^{-4} m/s while both 10^{-3} m/s (Figure 4.11) and 10^{-9} m/s (Figure 4.12) were used for the hydraulic conductivity of the borehole. The 2" and 12" borehole simulations are identical to the 4" borehole simulations (Figure 4.11 and 4.12). Thus, borehole size has no effect on LNAPL saturation in the borehole in this model.

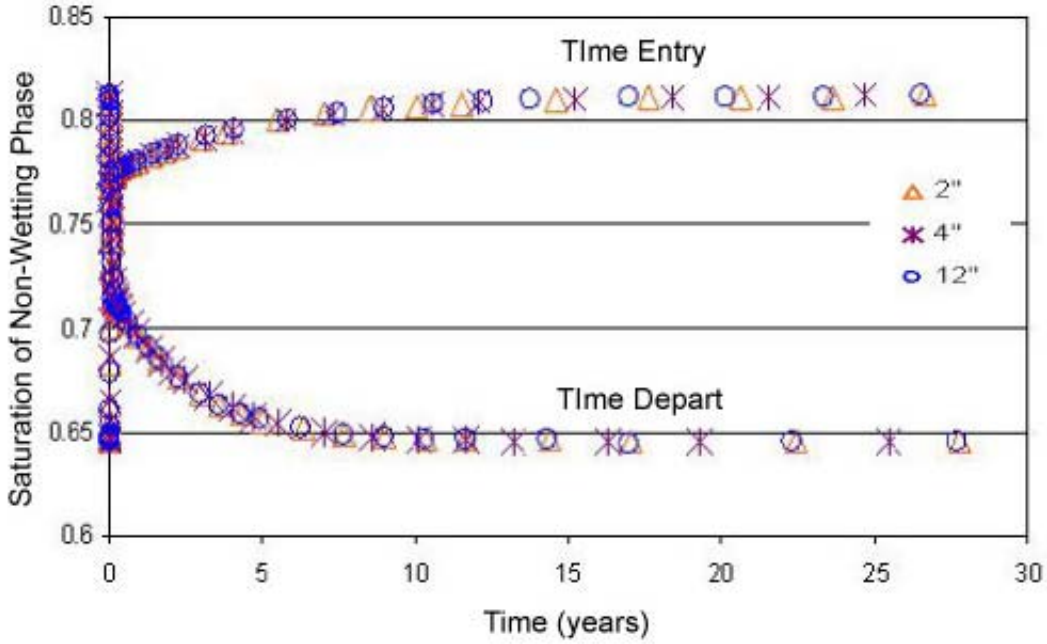

Figure 4.11: Saturation of the non-wetting phase in the center of 2, 4, and12 inch diameter boreholes (Borehole: K=10^{-3} m/s; Media: K= 10^{-4} m/s).

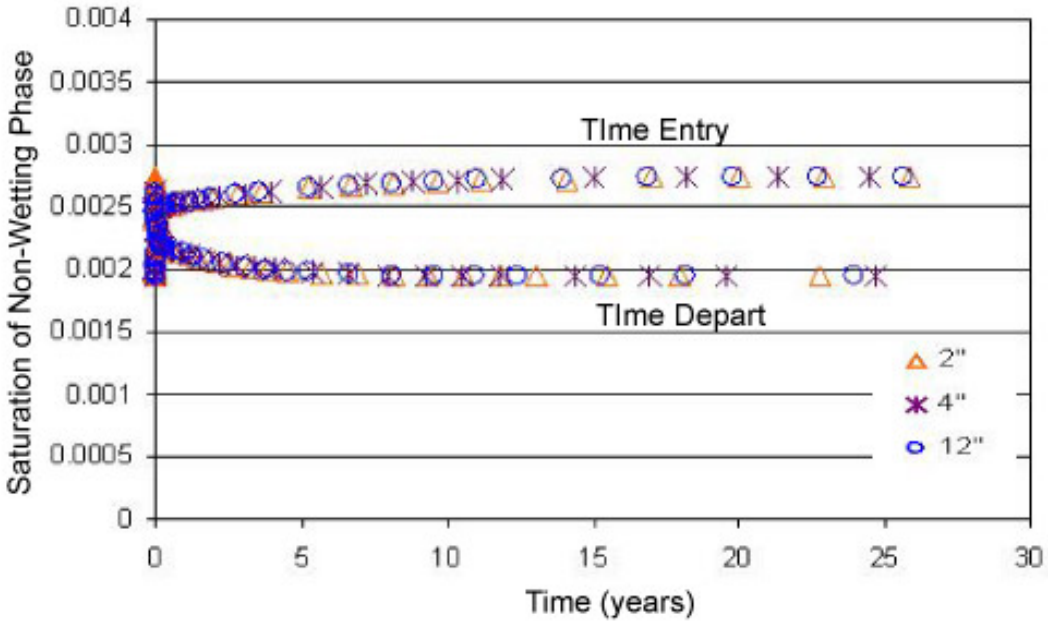

Figure 4.12: Saturation of the non-wetting phase in the center of 2, 4, and 12 inch diameter boreholes (Borehole: $K=10^{-9}$ m/s; Media: $K= 10^{-4}$ m/s).

The area of influence around the borehole did change for each borehole simulation. The original 4" borehole had an area of influence of approximately 0.5m. This decreased to 0.3 m from the 2" borehole and increased to 1 m from the 12" borehole. Thus, the capture zone of the borehole is affected by the size of the borehole as expected.

CHAPTER V

DISCUSSION

The field data collected from the Enid, Golden, and Hobart, OK sites will be compared to each other and to the modeling results. Implications from modeling results regarding the length of time in which a well and formation reach equilibrium in a two-phase system will be discussed. Finally, limitations to the application of the model results to field sites are addressed.

Comparison of Field and Model Results

The Enid site was the only field site where free product was observed in the monitoring wells (Figure 1.4), and was the only site that had monitoring wells located in a relatively uniform sand layer. However, these wells are not located in the plane of the resistivity images (Figure 1.3) but just north of the monitoring electrodes (Figure 1.2). LNAPL is likely converging into these wells due to pumping of the wells. Over time, LNAPL thickness in the monitoring wells decreased with the exception of one well (Figure 1.4). Decreased thickness of LNAPL in monitoring wells 17, 19, and 21 is mostly likely attributed to pumping efforts for remediation. The increase in product thickness in MW-18 is likely related to LNAPL coming from the south side of the site observed in ERI images and in core data collected in July to August 2003. The LNAPL coming on to the

site was a separate segment from the “plume” delineated during the initial site characterization.

The divergence from the electrode borings filled with bentonite may be partially due to the divergence effect modeled in this thesis. However, the effects observed in the COMSOL model were too small to explain the 2 – 3 m conductive regions on either side of the electrode wells. A higher gradient due to active pumping may explain the scale of the conductive regions, but has not been tested with the current model.

LNAPL thickness from wells at the Golden, OK site do not correlate with data from core sampling or ERI as the wells that correlated with ERI images had no detectable LNAPL. LNAPL blobs can be observed between the wells in electrical images (Figure 1.8). The presence of LNAPL was confirmed by soil borings (Halihan et al., 2005a). However, no free product was observed in the wells. The wells may not record free product since they were used for remediation (i.e., injection and extraction). Figure 1.8 shows LNAPL blobs moving toward to Well 16, which is an extraction well (Halihan et al., 2005a). LNAPL moves away from wells 48, 46, 52 and 50 because they are injection wells. Modeling results may not provide the mechanism to explain this site since a higher hydraulic gradient exists during remediation efforts. The observed scale of separation from the wells indicates that the modeled mechanism is not large enough to generate the LNAPL free zones around the wells.

An expected convergent flow field around the wells was not observed at the Hobart, OK site. The monitoring wells have filter packs consisting of 20/40

silica sand and the wells are sealed with bentonite chips above the screened intervals. The stratigraphy of this site (Table 1.3) predominantly consists of silty clay. Thus, the well has a higher hydraulic conductivity than the surrounding media which should cause a convergent flow field. From the modeling results, we would predict that the monitoring wells would be highly saturated with LNAPL (Figure 4.4). However, no hydrocarbon was measured in the monitoring wells. ERI and core data indicated that LNAPL contamination was present around the wells. A divergent flow field may be preventing LNAPL from entering the monitoring wells. Such a flow field could have been created by smearing when the well was drilled using an auger rig. As the well was drilled into the silty clay, the clay could have been smeared along the sides of the borehole. This would cause a skin effect which is preventing LNAPL migration into the well. The wells could have also been poorly developed which is causing the wells to not be open to surrounding media. An additional explanation provided by the COMSOL model is that the aquifer is not in equilibrium with the well as the model suggested that it may take several tens of years to reach equilibrium with the formation.

Overall, our model does not fully explain the reasons that LNAPL thickness measurements in wells do not correlate to ERI images and soil cores at these field sites. The model predicted convergent flow fields to be observed around wells at all of the sites. The field data did not correspond to the model prediction however, other factors such as high gradients due to pumping, poorly developed wells, and remediation efforts were at play. The model results do

indicate that the hydraulic conductivity contrast between the borehole and natural media is one more variable that may cause differences between LNAPL thickness measurements in wells and the surrounding media.

Equilibrium Time Scales

Our model did provide an estimate for the time equilibrium is reached between a borehole and the surrounding media in a two-phase system. Under an ambient hydraulic gradient, equilibrium is reached between 7 - 11 years after LNAPL was introduced into the system (Figure 5.1) at a small site of 50x50 meters. When LNAPL was forced to depart, the borehole equilibrium was reached from 5 - 7 years (Figure 5.1). Therefore, using an assumption of hydrostatic conditions may not be valid since the time in which equilibrium is reached under ambient gradients is longer than the time spent on typical site characterization and remediation projects. This indicates that hydrodynamic conditions within a borehole and surrounding media will never be reached, and transient conditions must be accounted for when correlating well data with formation data. For most sites, this data will not be available.

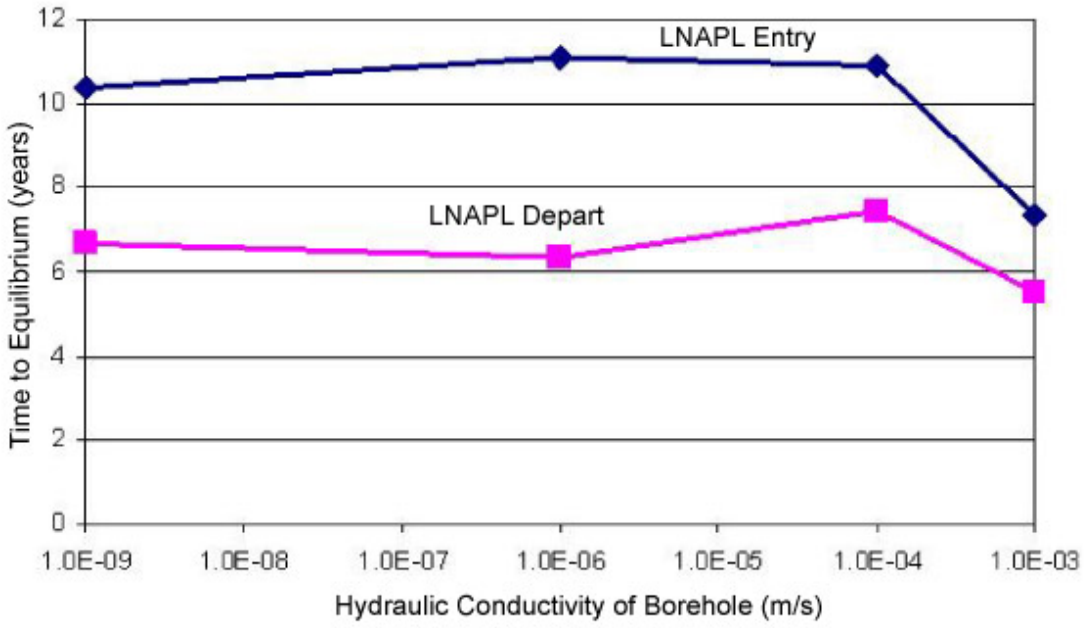

Figure 5.1: Time to equilibrium during the entry and departure of LNAPL. Hydraulic conductivity of the aquifer is 10^{-4} m/s. Log Scale.

Modeling Limitations

The numerical model had limitations in explaining the available field data.

1) The governing equations solve LNAPL saturation based on the pressure field. Since saturation is based on pressure instead of tracking the mass of the fluid, we were unable to examine any type of LNAPL ponding within the borehole. Examining the ponding effects of LNAPL in a borehole was not possible in this model, but may be a significant hydrodynamic effect in monitoring wells, especially in fine grained media.

2) Capture zones were small under low gradients (< 1 m). The model could not capture the scale of the zone as seen in resistivity images of several meters away from monitoring wells or electrode wells.

3) Monitoring wells were expected to read higher thicknesses of LNAPL in fine grained media. At our field sites, we did not detect LNAPL in contaminated areas from monitoring wells which may be due to a skin effect generated by auger rotation in a fine grained formation, or a lack of time to reach equilibrium which the model suggests may be years.

Future modeling efforts could be improved with saturation data from the field sites instead of only TPH data. Additionally, generating a model that calculated saturation through mass tracking equations instead of pressure equations may improve our understanding of monitoring well hydrodynamics.

CHAPTER VI

CONCLUSIONS

The major findings generated through the study of ERI, core samples, monitoring wells measurements and two-phase modeling:

1) Previous efforts to model the interaction of two-phase flow and monitoring wells indicate that wells are difficult to correlate to aquifer conditions under hydrostatic considerations. Factors affecting LNAPL thickness measurements in a well include multiphase interaction, capillary pressure, ground water table fluctuations, sediment variability, and pore size distribution.

2) Electrical resistivity imaging suggests that boreholes are interacting with the flow field. Resistive areas in ERI data that are correlated to the presence of LNAPL in the formation are either attracted to or repelled from monitoring points on a scale of several meters.

3) A hydraulic conductivity contrast between a borehole and surrounding porous media affect a two-phase flow field. When the hydraulic conductivity is greater in the borehole than the surrounding media a convergent flow field is formed. A divergent flow field is formed when the hydraulic conductivity of the borehole is less than the surrounding media.

This effect can lead to inaccurate LNAPL thickness measurements taken from a monitoring well.

4) Borehole modeling suggests hydrodynamic equilibrium may not be reached with the surrounding porous media. Model results show the time it can take for a borehole and the surrounding media to reach equilibrium can range from 9 to 23 years in an aquifer with a hydraulic conductivity of 10^{-4} m/s and even longer for lower conductivity materials.

5) Borehole modeling suggests that capture zones for monitoring wells or repulsion zones for installed electrode strings under ambient gradients are small, generally less than a meter. This suggests that a larger scale mechanism is required to explain ERI and core data.

REFERENCES

Adamski, M., Charbeneau, R.J., and Kuhn, J. 2007. LNAPL in the subsurface: recent developments, new conceptual models, and new tools. 19th Annual Tanks Conference & Expo, San Antonio, TX. p. 1-77.

Adamski, M., Kremesec, V., Kolhatkar, R., Pearson, C., and Rowan, B. 2005. LNAPL in fine-grained soils: conceptualization of saturation, distribution, recovery, and their modeling. Ground Water Monitoring & Remediation. 25:100-112.

Aestus, LLC. 2004. Report of GeoTrax Survey™ Work, Department of Human Health Services Site, Hobart, OK. p.1-27.

Aral, M.M., and Liao, B. 2002. Effect of groundwater table fluctuations on LNAPL thickness in monitoring wells. Environmental Geology. 42:151-161.

Atekwana, E.A., Sauck, W.A., Werkema Jr., D.D. 2000. Investigations of geoelectrical signatures at a hydrocarbon contaminated site. Journal of Applied Geophysics. 44:167-180.

Ballestero, T.P., Fiedler, F.R., and Kinner, N.E. 1994. An investigation of the relationship between actual and apparent gasoline thickness in a uniform sand aquifer. Ground Water. 32:708-718.

Beckett, G.D. and Huntley, D. 1998. Soil properties and design factors influencing free-phase hydrocarbon cleanup. Environmental Science and Technology. 32:287-293.

Benson, A.K. and Mustoe, N.B. 1996. DC resistivity, ground-penetrating radar, and soil and water quality data combined to assess hydrocarbon contamination: A case study in Arizona. Environmental Geosciences. 3:165-175.

Brooks, R.H. and Corey, A.T. 1964. Hydraulic properties of porous media. Hydrology, Paper 3, Colorado State University, Fort Collins, CO.

Carsell, R.F. and Parish, R.S. 1988. Developing joint probability distributions of soil water retention characteristics. Water Resources Research. 24:755-769.

Charbeneau, R.J. 2000. Groundwater Hydraulics and Pollutant Transport. Prentice Hall, New Jersey. p.1-594.

Charbeneau, R.J., Johns, R.T., Lake, L.W., and McAdams III, M.J. 1999. Free-Product Recovery of Petroleum Hydrocarbon Liquids. API Publication Number 4682. American Petroleum Institute, Washington, D.C. p.1.1-6.6.

Charbeneau, R.J., Johns, R.T., Lake, L.W., and McAdams III, M.J. 2000. Free-product recovery of petroleum hydrocarbon liquids. Ground Water Monitoring & Remediation. 20:147-158.

COMSOL Multiphysics. 2005. Earth Science Module; Model Library. 2:133-154.

Daily, W., Ramirez, A., LaBrecque, D., and Barber, W. 1995. Electrical resistance tomography experiments at the Oregon Graduate Institute. Journal of Applied Geophysics. 33:227-237.

de Marsily, Ghislain. 1986. Quantitative Hydrogeology: Groundwater Hydrology for Engineers. Academic Press, Inc., Florida.

Dahlberg, E.C. 1995. Applied Hydrodynamics in Petroleum Exploration. Springer-Verlag, New York. p.1-14.

Delaney, A.J., Peapples, P.R., and Arcone, S.A. 2001. Electrical resistivity of frozen and petroleum-contaminated fine-grained soil. Cold Regions Science and Technology. 32:107-119.

Driscoll, F.G. 1986. Groundwater and Wells. 2nd. ed. Johnson Filtration Systems Inc., St. Paul, Minnesota. p.438-483.

Farr, A.M., Houghtalen, R.J., and McWhorter, D.B. 1990. Volume estimation of light nonaqueous phase liquids in porous media. Ground Water. 28:48-56.

Fetter, C.W. 2001. Applied Hydrogeology. 4th. ed. Prentice Hall, New Jersey. p. 66-218.

Gleason, M.H., Daniel, D.E., and Eykholt, G.R. 1997. Calcium and sodium bentonite for hydraulic containment applications. Journal of Geotechnical and Geoenvironmental Engineering. 123:438-445.

Graham, I. 2007. Electrical Resistivity Imaging of a Remediated Gasoline Site in Golden, Oklahoma. Master of Science Thesis, Oklahoma State University, Stillwater, OK.

Grechka, V. and Soutter, L. 2005. Simulation of two-phase fluid flow through compactible reservoirs. Geophysical Prospecting. 53:829-841.

Halihan, T., Paxton, S., Graham, I., Fenstemaker, T., and Riley, M. 2005a. Post-remediation evaluation of a LNAPL site using electrical resistivity imaging. Journal of Environmental Monitoring. 7:283-287.

Halihan, T., Paxton, S., Graham, I., and Riley M. 2005b. Final report of activities for: Post remediation characterization of LNAPL using electrical resistivity and direct push techniques. Oklahoma Corporation Commission, Petroleum Storage Tank Division, Oklahoma City, OK. p.1-26.

Halihan, T., Paxton, S., McPhail, M., McSorley, J., and Riley, M. 2005c. Final report for: Environmental characterization and monitoring of LNAPL using electrical resistivity tomography (ERT) and hydraulic push techniques. Oklahoma Corporation Commission, Petroleum Storage Tank Division, Oklahoma City, OK. p.1-74.

Herzog, B.L. 1994. Slug tests for determining hydraulic conductivity of natural geologic deposits. *In* Daniel, D.E. and Trautwein, S.J. eds. Hydraulic Conductivity and Waste Contaminant Transport in Soil. 1994. American Society for Testing and Materials, Philadelphia, PA. p.95-110.

Huntley, D., Hawk, R.N., and Corley, H.P. 1994a. Nonaqueous phase hydrocarbon in a fine-grained sandstone: 1. Comparison between measured and predicted saturations and mobility. Ground Water. 32:626-634.

Huntley, D., Wallace, J.W., and Hawk, R.N. 1994b. Nonaqueous phase hydrocarbon in a fine-grained sandstone: 2. Effect of local sediment variability on the estimation of hydrocarbon volumes. Ground Water. 32:778-783.

Johnson, H.L. and Duchon, C.E. 1995. Atlas of Oklahoma Climate. University of Oklahoma Press, Norman, OK.

Kemblowski, M.W. and Chiang, C.Y. 1990. Hydrocarbon thickness fluctuations in monitoring wells. Ground Water. 28:244-252.

Kemna, A., Vanderborght, J., Kulessa, B., and Vereecken, H. 2002. Imaging and characterization of subsurface solute transport using electrical resistivity tomography (ERT) and equivalent transport models. Journal of Hydrology. 267:125-146.

LaBrecque, D.J., Ramirez, A.L., Daily, W.D., Binley, A.M., and Schima, S.A. 1996. ERT monitoring of environmental remediation processes. Measurement Science and Technology. 7:275-383.

Lenhard, R.J. 1990. Estimation of free hydrocarbon volume from fluid levels in monitoring wells; and, volume estimation of light nonaqueous phase liquids in porous media; discussion. Ground Water. 28:800-801.

Lenhard, R.J., and Parker, J.C. 1990. Estimation of free hydrocarbon volume from fluid levels in monitoring wells. Ground Water. 28:57-67.

Liao, B., and Aral, M.M. 1999. Interpretation of LNAPL thickness measurements under unsteady conditions. Journal of Hydrologic Engineering. p.125-134.

Loh, W.W., Waterfall, R.C., Cory, J., and Lucas, G.P. 1999. Using ERT for multi-phase flow monitoring. 1st World Congress on Industrial Process Tomography, Buxton, Greater Manchester. p.47-53.

McPhail, M.L. 2003. Geological Controls on the Location and Distribution of an LNAPL Plume at a Site in Enid, Oklahoma. Master of Science Thesis, Oklahoma State University, Stillwater, OK. p.1-137.

McSorley, J.D. 2003. Direct Push Electrical Resistivity Tomography to Detect NAPL. Master of Science Thesis, Oklahoma State University, Stillwater, OK. p.1-149.

Mualem, Y. 1976. A new model for predicting the hydraulic permeability of unsaturated porous media. Water Resources Research. 12:513-522.

Secor International Incorporated. 2004. Kiowa County Department of Human Services Final Report, Project No. 710T.08972.04.

Sleep, B.E., Sehayek, L., and Chien, C.C. 2000. A modeling and experimental study of light nonaqueous phase liquid (LNAPL) accumulation in wells and LNAPL recovery from wells. Water Resources Research. 36:3535-3545.

Thurston, R.N. 1974. Waves in solids. Encyclopedia of Physics, Mechanics of Solids. 4:109-302.

van Genuchten, M.T. 1980. A closed-form equation for predicting the hydraulic conductivity of unsaturated soils. Soil Science Society of America Journal. 44:892-898.

Vogler, M., Arslan, P., and Katzenbach, R. 2001. The influence of capillarity on multiphase flow within porous media: a new model for interpreting fluid levels in groundwater monitoring wells in dynamic aquifers. Engineering Geology. 60:149-158.

Wallace, J.W. and Huntley, D. 1992. Effect of local sediment variability on the estimation of hydrocarbon volumes. Ground Water Management. 11:273-285.

Weight, W.D. and Sonderegger, J.L. 2001. Manual of Applied Field Hydrogeology. McGraw-Hill. p.332-339.

APPENDIXES

APPENDIX A

LITHOLOGY AND WELL CONSTRUCTION AT HOBART, OK SITE

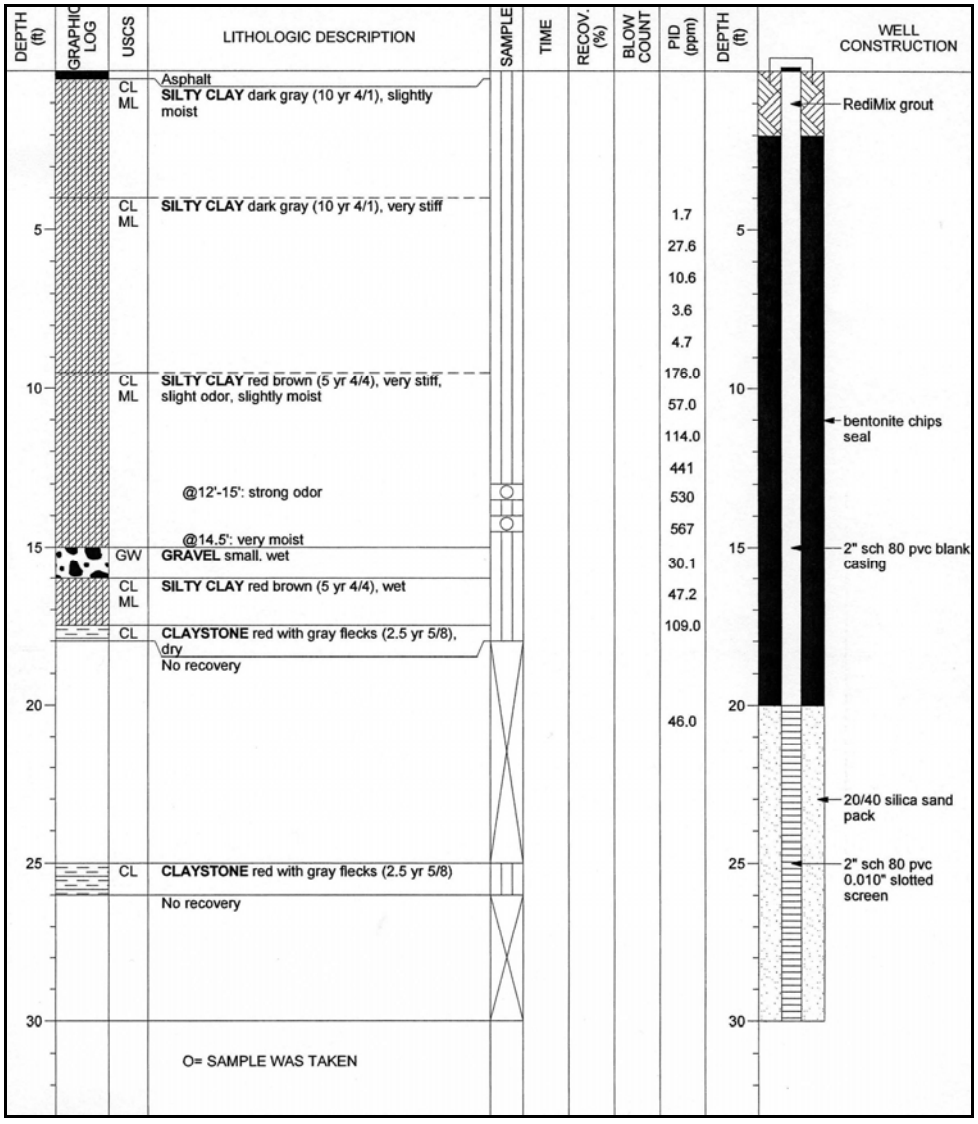

Lithology and well construction of MW-2 at Hobart, OK site (from Secor, 2004).

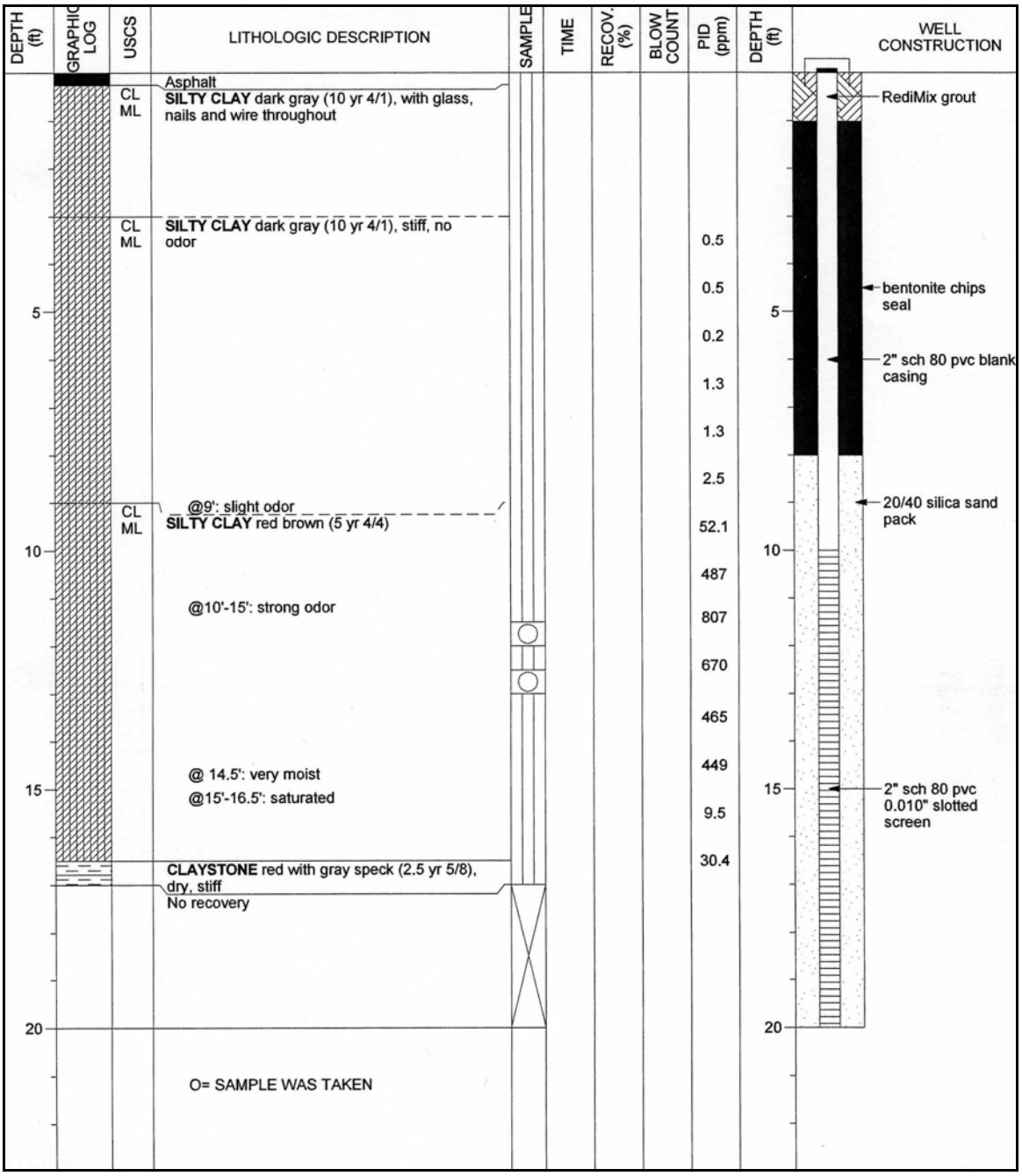

Lithology and well construction of MW-3 at Hobart, OK (from Secor, 2004).

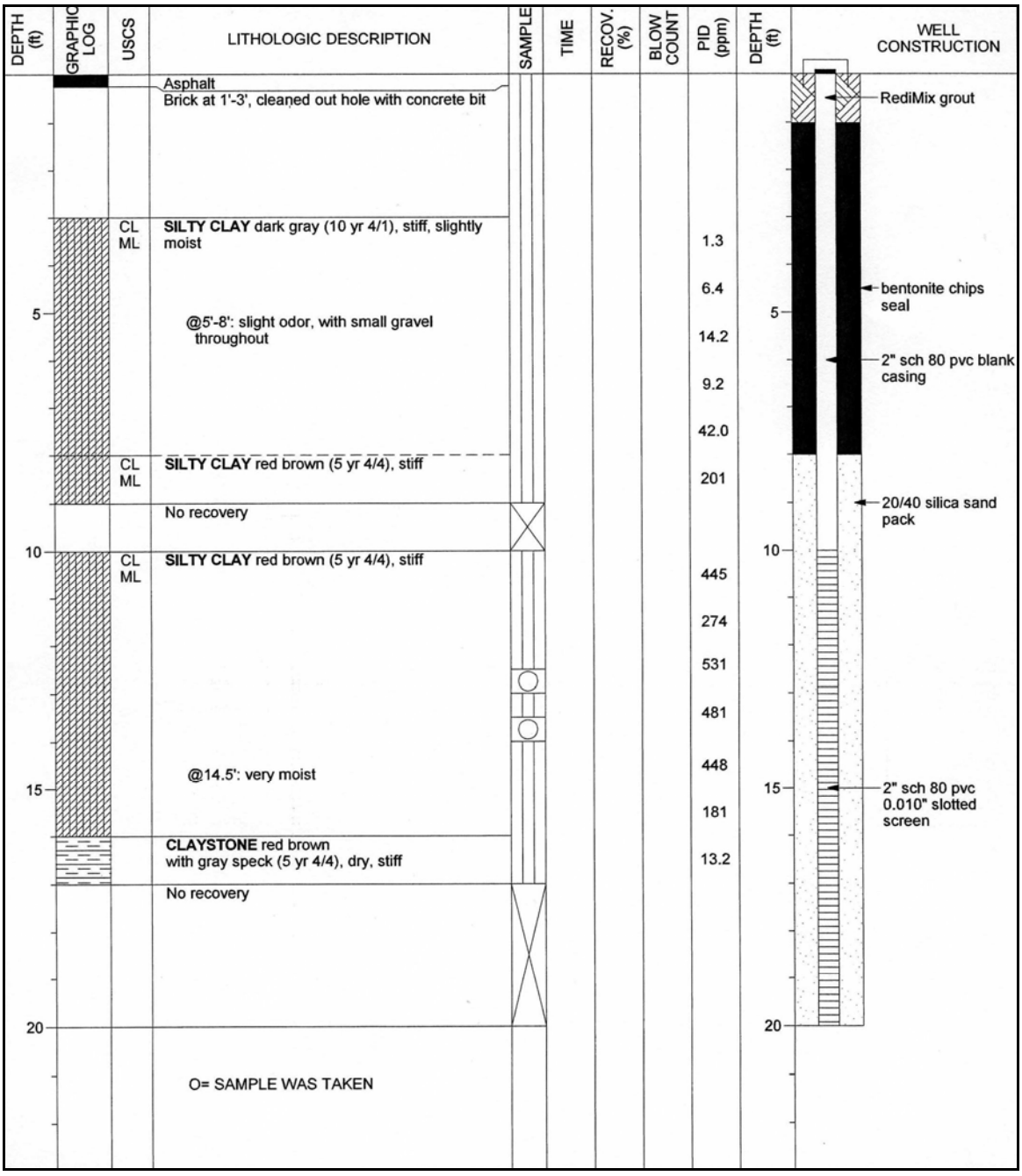

Lithology and well construction of MW-4 at Hobart, OK (from Secor, 2004).

APPENDIX B

COMSOL MULTIPHYSICS MODEL

COMSOL Multiphysics requires an extensive number of parameters to model two-phase flow. The program provides an output to be able to reproduce the model described in this thesis. This Appendix details the parameters used to generate the model.

1. Table of Contents

2. Model Properties

Property	Value
Model name	JT Thesis
Author	Jennifer Thorstad
Company	Oklahoma State University
Department	School of Geology
Reference	
URL	
Saved date	Apr 16, 2007 6:03:14 PM
Creation date	Mar 14, 2007 10:03:20 PM
COMSOL version	COMSOL 3.3.0.511

Application modes and modules used in this model:

- Geom1 (2D)
  - Darcy's Law (Earth Science Module)
  - Darcy's Law (Earth Science Module

3. Constants

Name	Expression	Value	Description
rhowater	1000		kg/m3
rhow	1000		kg/m3
etaw	0.001		
rhonw	800		kg/m3
etanw	0.000062		

4. Geometry

Number of geometries: 1

4.1. Geom1

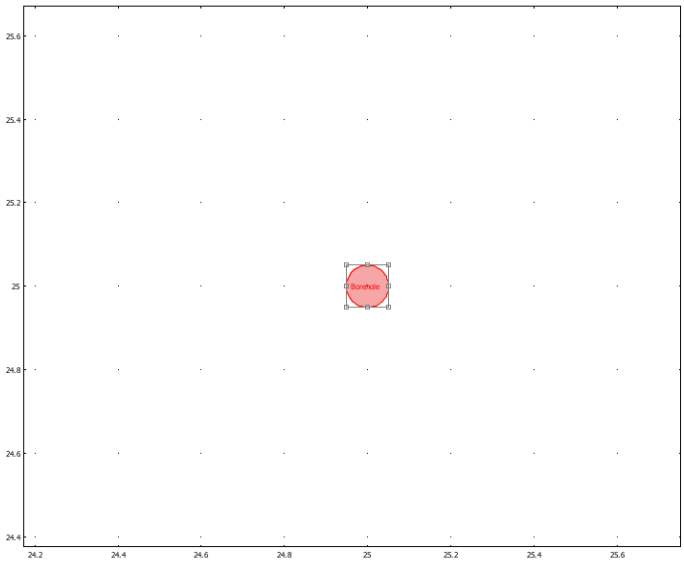

4.1.1. Point mode

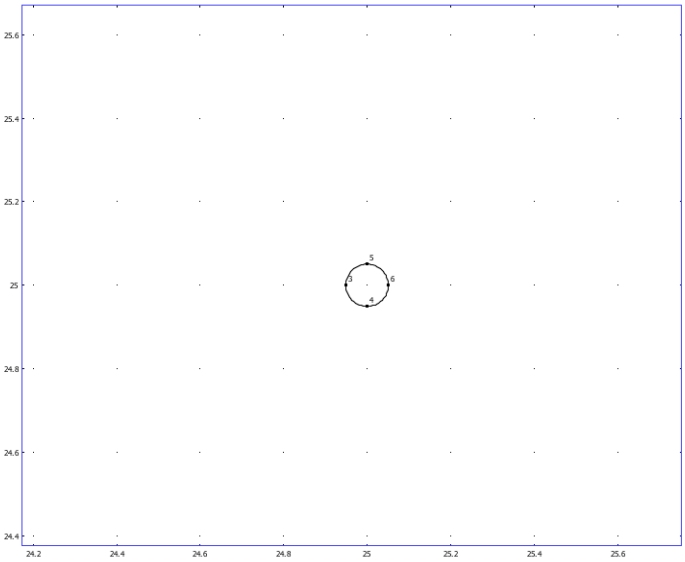

4.1.2. Boundary mode

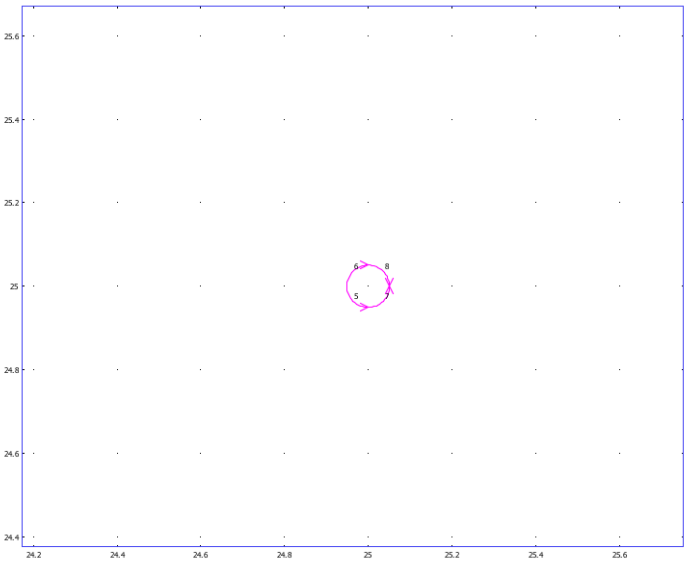

4.1.3. Subdomain mode

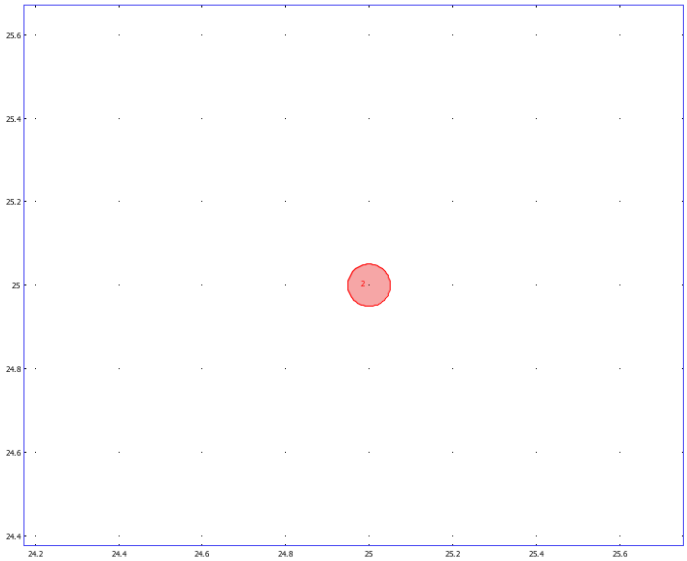

5. Geom1

Space dimensions: 2D

Independent variables: x, y, z

5.1. Scalar Expressions

Name	Expression
Cp	1/rhowater/g_w*((alpha*M/(1-M)*(thetas-thetar)*Sew^(1/M)*(1-Sew^(1/M))^M))*(Hc>0)
Hc	(pnw-pw)/(rhowater*g_w)
Sew	(1+abs(alpha*Hc)^N)^(-M)*(Hc>0)+1*(Hc<=0)
Senw	1-Sew
thetaw	(thetar+Sew*(thetas-thetar))*(Hc>0)+thetas*(Hc<=0)
thetanw	thetas-thetaw
krw	((Sew^L*(1-(1-Sew^(1/M))^M)^2)+eps)*(Hc>0)+1*(Hc<=0)
krnw	((1-Sew)^L*(1-Sew^(1/M))^(2*M))*(Hc>0)+eps
pw_in	9.82*x+18
pnw_in	1.1*x+1100

5.2. Expressions

5.2.1. Subdomain Expressions

Subdomain	1	2
thetas	0.43	0.36
thetar	0.045	0.07
kaps	1.02e-011	1.02e-016
alpha	14.44	0.49
N	2.68	1.09
M	1-1/N	1-1/N
L	0.5	0.5

5.3. Mesh

5.3.1. Mesh Statistics

Number of degrees of freedom	10098
Number of mesh points	1278
Number of elements	2494
Triangular	2494
Quadrilateral	0
Number of boundary elements	84
Number of vertex elements	8
Minimum element quality	0.734
Element area ratio	0

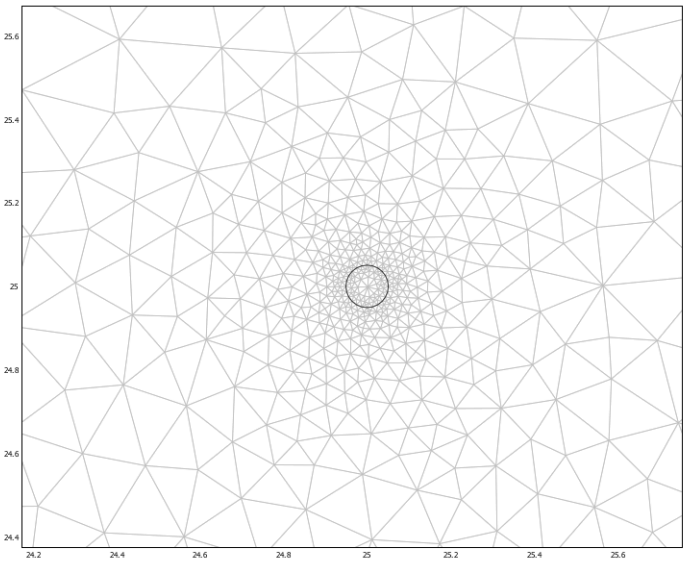

5.4. Application Mode: Darcy's Law (w)

Application mode type: Darcy's Law (Earth Science Module)

Application mode name: w

5.4.1. Scalar Variables

Name	Variable	Value	Description
tscale	tscale_w	1e-5	Heaviside scaling factor
g	g_w	9.82	Gravity
D	D_w	0	Elevation/vertical axis

5.4.2. Application Mode Properties

Property	**Value**
Default element type	Lagrange - Quadratic
Variable	Pressure analysis
Analysis type	Transient
Frame	Frame (ref)
Weak constraints	Off

5.4.3. Variables

Dependent variables: pw

Shape functions: shlag(2,'pw')

Interior boundaries active

5.4.4. Boundary Settings

Boundary		1	2-3
Type		Pressure	Zero flux/Symmetry
Pressure (p0)	Pa	**18**	0

Boundary	4	5-8
Type	Pressure	Continuity
Pressure (p0)	**509**	0

5.4.5. Subdomain Settings

Subdomain		1	2
Storage term (S)	1	**Cp**	**Cp**
Saturated hydraulic conductivity (Ks)	m/s	**1e-4**	**1e-9**
Saturated permeability (kaps)	m^2	**kaps*krw**	**kaps*krw**
Density-liquid (rhof)	kg/m^3	**rhow**	**rhow**
Viscosity-liquid (eta)	Pa·s	**etaw**	**etaw**

Subdomain initial value		1	2
Pressure (pw)	Pa	pw_in	pw_in

5.5. Application Mode: Darcy's Law (nw)

Application mode type: Darcy's Law (Earth Science Module)

Application mode name: nw

5.5.1. Scalar Variables

Name	Variable	Value	Description
tscale	tscale_nw	1e-5	Heaviside scaling factor
g	g_nw	9.82	Gravity
D	D_nw	0	Elevation/vertical axis

5.5.2. Application Mode Properties

Property	**Value**
Default element type	Lagrange - Quadratic
Variable	Pressure analysis
Analysis type	Transient
Frame	Frame (ref)
Weak constraints	Off

5.5.3. Variables

Dependent variables: pnw

Shape functions: shlag(2,'pnw')

Interior boundaries active

5.5.4. Boundary Settings

Boundary		1	2-3

Type		Pressure	Zero flux/Symmetry
Pressure (p0)	Pa	**983**	0

Boundary	4	5-8
Type	Pressure	Continuity
Pressure (p0)	**(Hpnw_t(t)*rhonw*g_nw)+1000**	0

5.5.5. Subdomain Settings

Subdomain		1	2
Storage term (S)	1	**Cp**	**Cp**
Saturated hydraulic conductivity (Ks)	m/s	**1e-3**	**1e-8**
Saturated permeability (kaps)	m^2	**kaps*krnw**	**kaps*krnw**
Density-liquid (rhof)	kg/m^3	**rhonw**	**rhonw**
Viscosity-liquid (eta)	Pa·s	**etanw**	**etanw**

Subdomain initial value		1	2
Pressure (pnw)	Pa	pnw_in	pnw_in

6. Interpolation Functions

6.1. Interpolation Function: Hpnw_t

Interpolation method: Linear

Data source type: Table

x	f(x)
0	.01
9.9999e9	.01
1e10	.05
2.9999e10	.05
3e10	.01
1e13	.01

7. Solver Settings

Solve using a script: off

Analysis type	Transient

Auto select solver	On
Solver	Time dependent
Solution form	General
Symmetric	auto
Adaption	Off

7.1. Direct (UMFPACK)

Solver type: Linear system solver

Parameter	Value
Pivot threshold	0.1
Memory allocation factor	0.7

7.2. Time Stepping

Parameter	Value
Times	0:1e9:1e11
Relative tolerance	0.004
Absolute tolerance	0.0005
Times to store in output	Time steps from solver
Time steps taken by solver	Free
Manual tuning of step size	Off
Initial time step	0.0010
Maximum time step	1.0
Maximum BDF order	5
Singular mass matrix	Maybe
Consistent initialization of DAE systems	Off
Error estimation strategy	Include algebraic
Allow complex numbers	Off

7.3. Advanced

Parameter	Value
Constraint handling method	Elimination
Null-space function	Automatic

Assembly block size	5000
Use Hermitian transpose of constraint matrix and in symmetry detection	Off
Use complex functions with real input	Off
Stop if error due to undefined operation	On
Type of scaling	None
Manual scaling	
Row equilibration	Off
Manual control of reassembly	Off
Load constant	On
Constraint constant	On
Mass constant	On
Damping (mass) constant	On
Jacobian constant	On
Constraint Jacobian constant	On

8. Postprocessing

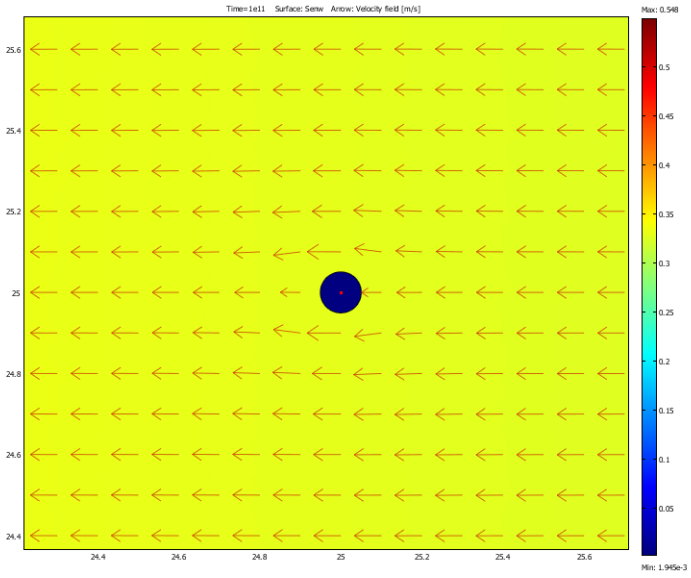

9. Variables

9.1. Point

Name	Description	Expression

rhof_w	Density	rhow
rhof_nw	Density	rhonw

9.2. Boundary

Name	Description	Expression
nU_w	Normal velocity	u_w * nx_w+v_w * ny_w
flux_w	Outward flux	u_w * nx_w+v_w * ny_w
nU_nw	Normal velocity	u_nw * nx_nw+v_nw * ny_nw
flux_nw	Outward flux	u_nw * nx_nw+v_nw * ny_nw

9.3. Subdomain

Name	Description	Expression
S_w	Storage term	Cp * CSs_w
Qs_w	Liquid source	0
K_w	Hydraulic conductivity tensor	Ks_w * CKs_w
Kxx_w	Hydraulic conductivity tensor	K_w
Kxy_w	Hydraulic conductivity tensor	0
Kyx_w	Hydraulic conductivity tensor	0
Kyy_w	Hydraulic conductivity tensor	K_w
kap_w	Permeability tensor	kaps_w * CKs_w
kapxx_w	Permeability tensor	kap_w
kapxy_w	Permeability tensor	0
kapyx_w	Permeability tensor	0
kapyy_w	Permeability tensor	kap_w
gradP_w	Pressure gradient	sqrt(pwx^2+pwy^2)

u_w	x-velocity	(-kapxx_w * (pwx+diff(rhof_w * g_w * D_w,x))-kapxy_w * (pwy+diff(rhof_w * g_w * D_w,y)))/eta_w
v_w	y-velocity	(-kapyx_w * (pwx+diff(rhof_w * g_w * D_w,x))-kapyy_w * (pwy+diff(rhof_w * g_w * D_w,y)))/eta_w
U_w	Velocity field	sqrt(u_w^2+v_w^2)
S_nw	Storage term	Cp * CSs_nw
Qs_nw	Liquid source	0
K_nw	Hydraulic conductivity tensor	Ks_nw * CKs_nw
Kxx_nw	Hydraulic conductivity tensor	K_nw
Kxy_nw	Hydraulic conductivity tensor	0
Kyx_nw	Hydraulic conductivity tensor	0
Kyy_nw	Hydraulic conductivity tensor	K_nw
kap_nw	Permeability tensor	kaps_nw * CKs_nw
kapxx_nw	Permeability tensor	kap_nw
kapxy_nw	Permeability tensor	0
kapyx_nw	Permeability tensor	0
kapyy_nw	Permeability tensor	kap_nw
gradP_nw	Pressure gradient	sqrt(pnwx^2+pnwy^2)
u_nw	x-velocity	(-kapxx_nw * (pnwx+diff(rhof_nw * g_nw * D_nw,x))-kapxy_nw * (pnwy+diff(rhof_nw * g_nw * D_nw,y)))/eta_nw
v_nw	y-velocity	(-kapyx_nw * (pnwx+diff(rhof_nw * g_nw * D_nw,x))-kapyy_nw * (pnwy+diff(rhof_nw * g_nw * D_nw,y)))/eta_nw
U_nw	Velocity field	sqrt(u_nw^2+v_nw^2)

VITA

Jennifer L. Thorstad

Candidate for the Degree of

Master of Science

Thesis: INFLUENCE OF BOREHOLE CONSTRUCTION ON LNAPL THICKNESS MEASUREMENTS

Major Field: Geology

Biographical:

Personal Data: Born on April 17, 1983 in Alexandria, MN. Grew up east of Hoffman, MN.

Education: Graduated from West Central Area Secondary Schools, Barrett, MN in May 2001. Received Bachelor of Science in Geology from North Dakota State University, Fargo, ND in May 2005. Completed the requirements for the Master of Science degree in Geology at Oklahoma State University in May 2007.

Experience: Employed by Oklahoma State University School of Geology as a teaching assistant from 2005 to 2007.

Professional Memberships: Geological Society of America

Name: Jennifer L. Thorstad Date of Degree: May, 2007

Institution: Oklahoma State University Location: Stillwater, Oklahoma

Title of Study: INFLUENCE OF BOREHOLE CONSTRUCTION ON LNAPL THICKNESS MEASUREMENTS

Pages in Study: 84 Candidate for the Degree of Master of Science

Major Field: Geology

Abstract: Electrical resistivity images taken at sites contaminated by gasoline or light non-aqueous phase liquids (LNAPL) often image LNAPL being affected by the location of boreholes as either an attractive or repulsive feature in the subsurface. This mechanism results in an anomalously low or high estimate of the amount of LNAPL in the formation using data sampled from wells. The field data suggest that in fine grained media LNAPL may not be detected by monitoring wells. A numerical model was constructed to determine if the hydraulic conductivity contrast between a borehole and natural media has a significant enough effect to create either a convergent or divergent two-phase flow field around a borehole which would lead to inaccurate LNAPL measurements. The model results indicate that ambient gradients are not sufficient to create the observed geophysical effect, but do demonstrate that the wells may never reach equilibrium with the formation.

ADVISOR'S APPROVAL: Dr. Todd Halihan